



Research Paper

CuO nanoparticles supported by ceria for NO_x-assisted soot oxidation: insight into catalytic activity and sintering



Tahrizi Andana ^{a,b}, Marco Piumetti ^a, Samir Bensaid ^{a,*}, Laurent Veyre ^b, Chloé Thieuleux ^b, Nunzio Russo ^a, Debora Fino ^a, Elsje Alessandra Quadrelli ^b, Raffaele Pirone ^a

^a Department of Applied Science and Technology, Politecnico di Torino, Corso Duca degli Abruzzi 24, 10129, Turin, Italy

^b Université de Lyon 1, ICL, C2P2 UMR 5265, CPE Lyon, 43 Bd du 11 Novembre 1918, F-69616 Villeurbanne, France

ARTICLE INFO

Article history:

Received 6 February 2017

Received in revised form 15 May 2017

Accepted 20 May 2017

Available online 22 May 2017

Keywords:

Ceria

CuO nanoparticles

Organosilane

Oxidations

Soot

NO_x

Sintering

ABSTRACT

The current work introduces Cu nanoparticles (Cu-NPs) stabilized by organosilane and deposited as CuO-NPs onto ceria with two different morphologies: spongy, microstructured ceria synthesized by Solution Combustion (CeO₂-SCS) and nanostructured ceria nanocubes (CeO₂-NC). Catalytic activity tests have demonstrated that combination of CuO-NPs and CeO₂-SCS bring significance to CO and NO oxidations as it results in easier reducibility and better metal dispersion on the surface. However, CuO-NPs with CeO₂-NC give the opposite effect on CO and NO oxidations: the increase of Cu loading lowers the catalytic activity. However, Cu/CeO₂-NC combination, especially the one with low Cu loading, gives the best synergy for normal soot oxidation with oxygen, thanks to the structure-sensitivity of the reaction. In the presence of NO_x, Cu/CeO₂-SCS catalysts are active for soot oxidation at low temperature as the catalysts favor early NO₂ formation. Lastly, a series of repeated tests with NO_x-assisted soot oxidation was carried out to confirm that CuO-NPs suffer easily from particle sintering, possibly via migration and coalescence.

© 2017 Elsevier B.V. All rights reserved.

1. Introduction

Unconventional abatement of particulate matter (PM), or more commonly known as “soot”, in the exhaust gas stream of Diesel cars has been developed worldwide in response to increasing global demands for more efficient and safer soot oxidation. Current approach seeks to make use of noxious gases as the secondary oxidizing agent, since they are produced more abundantly in Diesel cars than in their gasoline counterparts. NO₂, in particular, is a radical chemical compound that oxidizes more powerfully than oxygen, thus allowing early initiation of soot oxidation. However, in the exhaust gas stream NO₂ exists in a lower quantity than its reducing pair, NO. This automatically prescribes an active oxidation catalyst able to mediate conversion of NO to NO₂ at the lowest temperature possible.

Noble metals undoubtedly come in handy when it comes to improving the activity of gas-phase oxidation reactions. Platinum (Pt) is one of the most exploited metals for boosting the abatement

activity of pollutants, such as CO and hydrocarbons in Three-Way Catalysis (TWC) [1–3] and NO to NO₂ in Lean NO_x Trap (LNT) [4,5]. The metal is far-famed for its ability to easily attract and further dissociate dioxygen into two oxygen adatoms [6]. These atoms subsequently migrate to the catalyst support via spillover phenomena and eventually become available for surface reaction with pollutants [7,8]. Regardless the excellency, the commercial use of Pt is rather limited due to economic reasons. Pt also suffers frequently from poisoning, such as by CO [9,10] and severely by sulfur oxides (SO_x) that unluckily exist as byproducts of sulfurous Diesel fuel combustion [11,12]. Amongst non-precious transition metals ever investigated in automotive catalysis, copper (Cu) is of particular interest. Cu has been employed in many investigations as a catalyst for selective NO_x reduction [13–15], N₂O decomposition [16,17], CO oxidation [18–20] and soot oxidation [21,22]. Cu is a polyvalent metal; it exists in these three possible oxidation states, namely Cu(0), Cu(I) and Cu(II). Its oxide form, which normally exists as CuO, promotes Mars-van Krevelen (MvK)-like reduction/oxidation mechanism on the surface, which has been found to be essential in oxidation reactions [23,24]. Similar to Pt, Cu can also improve oxidation reaction by activating oxygen molecules on the surface and subsequently mediating the oxygen spillover to the support

* Corresponding author.

E-mail address: samir.bensaid@polito.it (S. Bensaid).

[25]. The use of Cu, in addition, benefits from its inherent SO₂-resistant nature. It has been reported elsewhere that even under high concentration of SO₂ Cu does not suffer from deactivation [26].

Reduction in the particle size improves the metal dispersion. The preparation of metal nanoparticles can be achieved by introducing steric stabilization created by an organometallic compound [27]. The organometallic ligands keep the particles from agglomerating and eventually maintains a small dimension. Pelzer et al. have brought out the application of organosilane to Ru(COT)(COD) and Pt(dba)₂ that resulted in small well-defined Ru and Pt nanoparticles (± 2 nm) [28,29]. Boualleg et al. have prepared silane-stabilized Pt and Pt₃Sn nanoparticles and incorporated them into channel pores of mesostructured silica [30,31]. Baudouin et al. have applied the same method for stabilizing 2-nm Ni nanoparticles from Ni(COD)₂ precursor and have demonstrated the resistance of the metals to sintering [32]. Likewise, we have previously prepared similar Pt and Pt₃Sn nanoparticles that promote high catalytic activities with CO and NO_x-assisted soot oxidations [33]. In addition, we have also demonstrated that our Pt-NPs still performed well even after having been aged thermally at 700 °C for 8 h [33].

In the context of automotive catalysis, ceria (CeO₂) has been extensively investigated as the catalyst support mainly due to its ability to undergo quick redox reactions [34–37]. Ceria on nanoscale, depending on the type of the precursor and the preparation, is tailorable into various well-defined morphologies, such as nanopolyhedra, nanorods and nanocubes; each has a discernible catalytic activity towards several reactions [38–42]. CO oxidation has been frequently employed as the probe reaction in several investigations. It has been found that (100) plane that exists in ceria nanorods and, more predominantly, in ceria nanocubes is responsible for the high catalytic activity of ceria towards CO oxidation [41,43,44]. Soot oxidation on nanostructured ceria has also been reportedly structure-sensitive, which means that the catalytic activity is dependent on morphology [40,42,45,46]. Nanocubes are by far the best morphology for soot oxidation, thanks to the abundance of (100) surfaces, over which formation of oxygen vacancies is lower compared to that over (110) surface [44,47].

Binary CuO-CeO₂ system has been attracting many researchers in years due to its superior catalytic activity towards several reactions, such as CO oxidation [20,48–50], VOC oxidation [48,49,51] and N₂O decomposition [52,53]. The excellent reactivity of this system stems from the synergistic effect between CuO and CeO₂ that allows coupled redox cycles between Ce³⁺/Ce⁴⁺ and Cu²⁺/Cu⁺, enhances the number of defective sites (e.g. oxygen vacancies) and improves ceria reducibility [17,48,54–56]. In addition, soot oxidation equally benefits this synergism. Previous work has demonstrated that mixing CuO and CeO₂ (prepared by solution combustion synthesis) at Cu/Ce atomic ratio of 5/95 resulted in an active material that gives the lowest $T_{50\%}$ of soot combustion [48]. The presence of CuO can also enhance the oxidation of NO to NO₂, leading to more enhanced NO_x-assisted soot oxidation [57,58].

Introduced herein are Cu nanoparticles (Cu-NPs) synthesized by using *n*-octylsilane as the stabilizer and mesitylcopper (I) as the precursor [59]. The stabilized Cu-NPs were deposited onto two morphologically different ceria supports. The work has been systematically carried out as follows: (1) characterizations of the prepared catalysts for determination of textural and morphological properties and surface electronic properties, and (2) catalytic activity tests for discerning the roles of CuO and the ceria support in several oxidation reactions. The reactions investigated in this work are: (1) CO oxidation as an intermediate reaction in soot oxidation reaction mechanism; (2) NO oxidation as the reaction that exploits the functionality of CuO; (3) NO_x-free soot oxidation and (4) NO_x-assisted soot oxidation as core reactions in this work.

2. Experimental

2.1. Synthesis

Cu-NPs (0.16 mmol) is typically obtained by mixing mesitylcopper (I) (0.16 mmol, STREM Chemicals) and *n*-octylsilane (0.16 mmol, Sigma-Aldrich) in a Schlenk flask containing anhydrous THF (28.7 ml, Sigma-Aldrich). Upon the addition of *n*-octylsilane, the colorless mesitylcopper (I) solution in THF turns gradually into a black colloid. The mixture is then transferred into a high-pressure glass reactor and mildly reduced with 3 barg of H₂ overnight.

CeO₂-SCS (SCS=solution combustion synthesis) and CeO₂-NC (NC=nanocubes) as the catalyst supports were prepared via solution combustion and hydrothermal syntheses respectively. CeO₂-SCS is typically synthesized by dissolving 1.9 g of Ce(NO₃)₃·6H₂O (Sigma-Aldrich) and 0.8 g of urea (Sigma-Aldrich) in 60 ml of deionized water. The solution is then poured into a ceramic crucible, heated in a furnace at 650 °C for 20 min. On the other hand, CeO₂-NC has been prepared according to the literature [45]. The synthesis typically begins with mixing 4.4 g of Ce(NO₃)₃·6H₂O and 48 g of NaOH in 80 ml of deionized water. The violetish-white slurry resulting from the precipitation is then transferred into a 200-ml autoclave, treated at 180 °C for 24 h. The white precipitate is rinsed with ethanol and deionized water, separated from the washing liquid in a centrifuge and dried overnight at 70 °C. The final solid is calcined at 550 °C for 4 h.

Two different theoretical Cu loadings with respect to the weight of the support, 1% and 5%, were used to study the effect of Cu loading on the oxidation reactions. Metal loading is typically done via wetness impregnation (WI) technique according to this following procedure: the final black Cu colloid is initially concentrated via vacuum evaporation to reach the adequate impregnation volume. The concentrated colloid is transferred dropwise onto the support under flowing Ar. The wet support is left exposed to ambient air overnight to allow drying process. CuO-NPs/CeO₂ system is finally obtained after having air-dried the impregnated support at 120 °C for 2 h to remove the remaining solvent and calcined at 320 °C for 10 h to remove the ungrafted ligands.

2.2. Characterization

N₂ physisorption analysis was carried out in a Tristar II 3020 Micromeritics instrument to determine BET surface areas and pore volumes of the prepared catalysts. Before the analysis, the catalysts were pre-heated at 200 °C for 2 h under vacuum. The specific surface area was finally calculated via BET method, and is thus denoted herein as S_{BET} . The copper content in the samples was analyzed via an inductively coupled plasma atomic emission spectroscopy (ICP-AES) at Politecnico di Torino, Italy.

X-ray diffractograms were recorded on an X'Pert Philips PW3040 diffractometer using Cu K α radiation. The intensity data were collected over a 2 θ range of 20–70° with a 0.013° step size and using a counting time of 0.2 s per step. The diffraction peaks were identified using powder diffraction files by International Centre of Diffraction Data (ICDD). Particle size was estimated by applying Scherrer's equation, in which the FWHM data were corrected with respect to those of lanthanum hexaboride (instrument calibration standard).

Sample morphology was observed via transmission electron microscopes [TEM, Jeol JEM-3010, 300 kV Ultrahigh resolution, Università degli Studi di Torino and HRTEM JEOL 2100FEG (field emission gun) microscope at the "Centre Technologique des Microstructures", CT μ , Villeurbanne, France]. Element mapping with EDX was carried out via Oxford Instruments by INCA.

X-ray photoelectron spectroscopy was performed in a PHI Versa probe apparatus using a band-pass energy of 187.85 eV, a 45° take off angle and a 100.0 μm diameter X-ray spot size. Ce, O and Cu oxidation states on the surface were eventually interpreted from the deconvoluted spectra.

The reducibility of the catalysts was analyzed by means of H₂-TPR (temperature-programmed reduction) in a Thermo Scientific TPDRO 1100 instrument. The analysis was carried out by sending continuously 5%-vol H₂ in Ar at a rate of 20 ml min^{-1} to 0.1 g of catalyst while the oven temperature increases from 30 °C to 900 °C at a rate of 10 °C min^{-1} . The H₂O signal was detected by TCD (thermal conductivity detector).

2.3. Catalytic activity tests

A setup for catalytic activity tests is generally composed of a PID-regulated furnace, a quartz U-tube reactor with a fixed catalytic bed on one side, a K-type thermocouple placed in such a way that its tip is as near as possible to the bed, a non-dispersive infrared (NDIR) continuous gas analyzer (ABB Uras 14) for CO and CO₂ detection and an Emerson XStream X2GP gas analyzer for NO, NO₂ and O₂ detection. The reactor is also equipped with bypass line, in which main gases like CO and NO initially flow to fix the concentrations at their desired values. The catalytic beds and the test's sequences are dependent on type of the test and the details about them are presented below:

a.) CO oxidation

In this test, 100 mg of catalyst is used as the catalytic bed. Prior to the main reaction, the catalyst is pre-heated at 100 °C for 30 min under 50 ml min^{-1} of air. The reactor is then cooled at a rate of 5 °C min^{-1} to 50 °C. During the cooling process, a mixture of 1000 ppmv CO and 10%-v O₂ in N₂ is sent at a rate of 50 ml min^{-1} in bypass line. After the gas saturation, the flow is sent back to the reactor and the gradual heating starts at a rate of 5 °C min^{-1} . The test proceeds until the temperature reaches 300 °C.

b.) NO oxidation

In this test, a mixture of 150 mg of SiO₂ (Umicore) and 45 mg of catalyst (gently stirred with spatula for 3 min) is used as the catalytic bed. Prior to the main reaction, the catalyst is pre-heated at 100 °C for 30 min under 100 ml min^{-1} of 20%-v O₂ in N₂. The reactor is then cooled at a rate of 5 °C min^{-1} to 50 °C. During the cooling process, a mixture of 550 ppmv NO and 10%-v O₂ in N₂ is sent at a rate of 100 ml min^{-1} in bypass line. After the gas saturation, the flow is sent back to reactor and the gradual heating starts at a rate of 5 °C min^{-1} . The test proceeds until the reactor temperature is at 650 °C.

Table 1
Textural properties of the catalysts.

Sample	S_{BET} ($\text{m}^2 \text{g}^{-1}$) ^a	V_p ($\text{cm}^3 \text{g}^{-1}$) ^a	D_p (nm) ^b	Cu content	
				(%wt) ^c	$\mu\text{mol g cat}^{-1}$
1% Cu/CeO ₂ -SCS	36	0.03	14	0.90	142
5% Cu/CeO ₂ -SCS	35	0.03	14	2.94	463
1% Cu/CeO ₂ -NC	9	0.04	118	0.89	140
5% Cu/CeO ₂ -NC	18	0.05	94	3.17	499
CeO ₂ -SCS	38	0.04	14	–	–
CeO ₂ -NC	8	0.07	90	–	–

^a Obtained from N₂ physisorption.

^b Calculated via Scherrer's equation.

^c Obtained from ICP-AES analysis.

c.) NO_x-free soot oxidation

In this test, a loose mixture of 150 mg of SiO₂ (Umicore), 5 mg of model soot (Printex-U from Degussa) and 45 mg of catalyst (gently stirred with spatula for 3 min) is used as the catalytic bed. Prior to the main reaction, the catalyst is pre-heated at 100 °C for 30 min under 100 ml min^{-1} of N₂. The oxidizing stream containing 10%-v O₂ in N₂ is sent at a rate of 100 ml min^{-1} directly to reactor. The gradual heating proceeds afterwards at a rate of 5 °C min^{-1} from ambient temperature to 700 °C.

d.) NO_x-assisted soot oxidation

In this test, a loose mixture of 150 mg of SiO₂ (Umicore), 5 mg of model soot (Printex-U from Degussa) and 45 mg of catalyst (gently stirred with spatula for 3 min) is used as the catalytic bed. Prior to the main reaction, the catalyst is pre-heated at 100 °C for 30 min under 100 ml min^{-1} of 20%-v O₂ in N₂. The reactor is then cooled at a rate of 5 °C min^{-1} to 50 °C. During the cooling process, a mixture of 550 ppmv NO and 10%-v O₂ in N₂ is sent at a rate of 100 ml min^{-1} in bypass line. After the gas saturation, the flow is sent back to reactor and the gradual heating starts at a rate of 5 °C min^{-1} . The test proceeds until the reactor temperature is at 700 °C.

e.) Catalyst stability

In the test of catalyst stability, NO_x-assisted soot oxidation is used as the probe reaction. Therefore, the reaction condition and the test sequence elaborated previously in Point d are employed. However, in this test the reaction is repeated twice with the used catalyst.

3. Result and discussion

3.1. Textural properties of the catalysts

Table 1 summarizes the BET surface areas and pore volumes for all samples derived from N₂ physisorption analysis. Ceria nanocubes (CeO₂-NC), as reported frequently elsewhere [40,43,45], has a very low surface area ($S_{\text{BET}} = 8 \text{ m}^2 \text{ g}^{-1}$) that is about one fifth of the surface area of the CeO₂-SCS ($S_{\text{BET}} = 38 \text{ m}^2 \text{ g}^{-1}$) sample. Low surface area translates into low amount of interparticle voids in the sample. This is a typical characteristic of nanocubic particles as their chiseled geometry and large dimension do not confer microstructures and porosity. As observed on **Table 1**, the impregnation of CeO₂-SCS with Cu-NPs generally leads to minor changes in textural properties. This is most likely due to the fact that both CuO-NPs and CeO₂-SCS share a similar granulometry, that is spherical with small particle size. On the other hand, the impregnation of CeO₂-NC with CuO-NPs results in high BET surface area at high metal loading (5%-wt Cu). Analysis with ICP-MS has estimated that the Cu con-

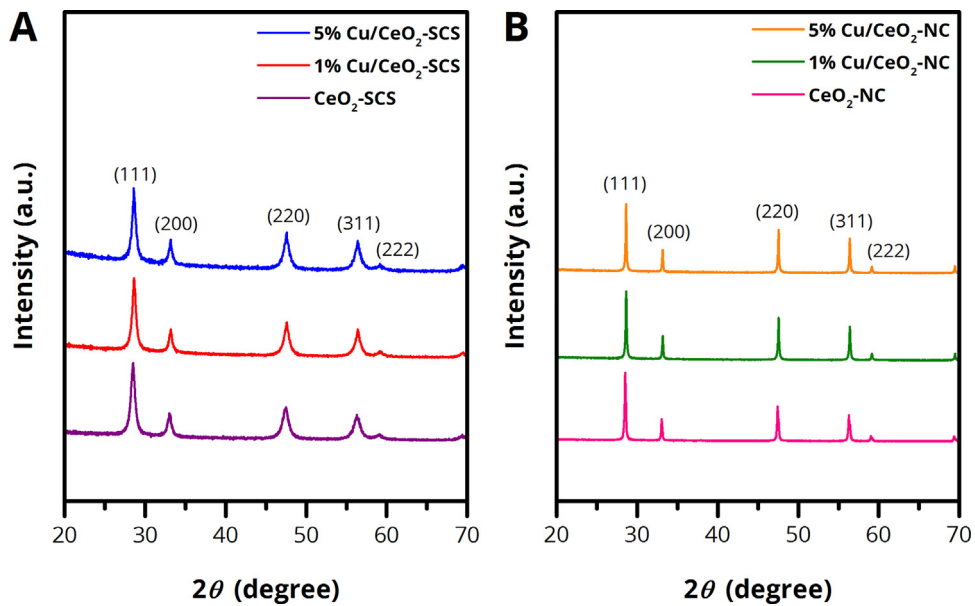


Fig. 1. X-ray diffractogram of (A) SC-synthesized and (B) nanocubic catalysts.

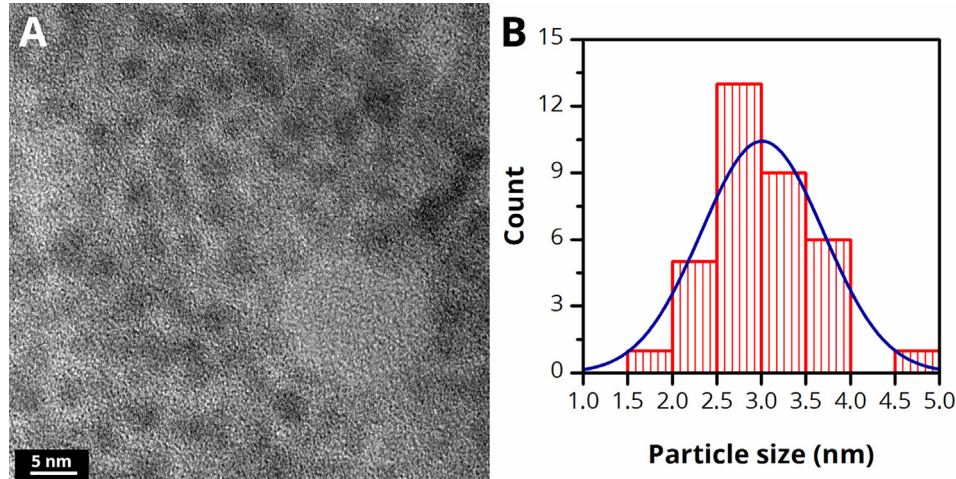


Fig. 2. TEM image of colloidal Cu-NPs (A) and their corresponding particle size distribution (B).

tent in 1% Cu/CeO₂ samples is about 0.9%-wt while in 5% Cu/CeO₂ samples is around 3%-wt.

Fig. 1 shows the X-ray diffractogram of the prepared catalysts. Fig. 1A shows the diffractograms of SC-synthesized catalysts while Fig. 1B shows those of nanocubic catalysts. Irrespective of the morphology, all diffractograms show five identical peaks (at similar positions). The peaks are characteristic of CeO₂ (ICDD JCPDS Ref No. 00-034-0394) and ascribed further to (111), (200), (220), (311) and (222) planes [40,45]. No suspicious peaks of CuO appear between 2θ range of 35° and 45° in the diffractograms of Cu-containing catalysts. Comparison between the two series of catalysts has shown that the peaks of SC-synthesized catalysts are broad while those of nanocubic catalysts are rather narrow. Table 1 also summarizes the estimated crystallite size of the catalysts calculated via Scherrer's equation. It is observed that the SC-synthesized catalysts are much smaller in size (ca. 14 nm) than nanocubic catalysts (90–100 nm). We have previously reported the micrography analysis of SC-synthesized and nanocubic ceria via FE-SEM [43,45,46], from which we have observed that the SC-synthesized ceria was microstructured but composed of a network of small nanoparti-

cles (around 10 nm) while nanocubic ceria had an average size of 100–300 nm.

Fig. 2 shows the TEM image of colloidal Cu-NPs (Fig. 2A) as well as its corresponding particle size distribution (Fig. 2B). It appears that the applied synthesis results in nanoparticles whose dimension ranges from 2 to 4 nm. The distribution is somewhat less narrow than that of Pt-NPs prepared with the same method [28,33]. Fig. 3A and B show the TEM images of the Cu-impregnated catalysts. The micrographs (a) and (b) on Fig. 3A show the images of 1% Cu/CeO₂-SCS. SC-synthesized catalysts are typically observed via TEM as microstructures that are rich with particle agglomerates. On the two figures, few dark spots appear on the thin surfaces and can thus be ascribed to CuO-NPs. It is very important to understand that CuO-NPs hardly appear in a great contrast with ceria since copper is substantially lighter than cerium. The micrograph (a) on Fig. 3B provides more TEM images of this sample, on which CuO-NPs with the average size of 5 nm appears with a very low contrast on a thin ceria surface. The particle size after the impregnation seem slightly larger than that in the colloidal solution, possibly due to calcination, although particles with small dimension are still visible. Better observation of CuO-NPs is obtained on 5% Cu/CeO₂-SCS [Fig. 3A,

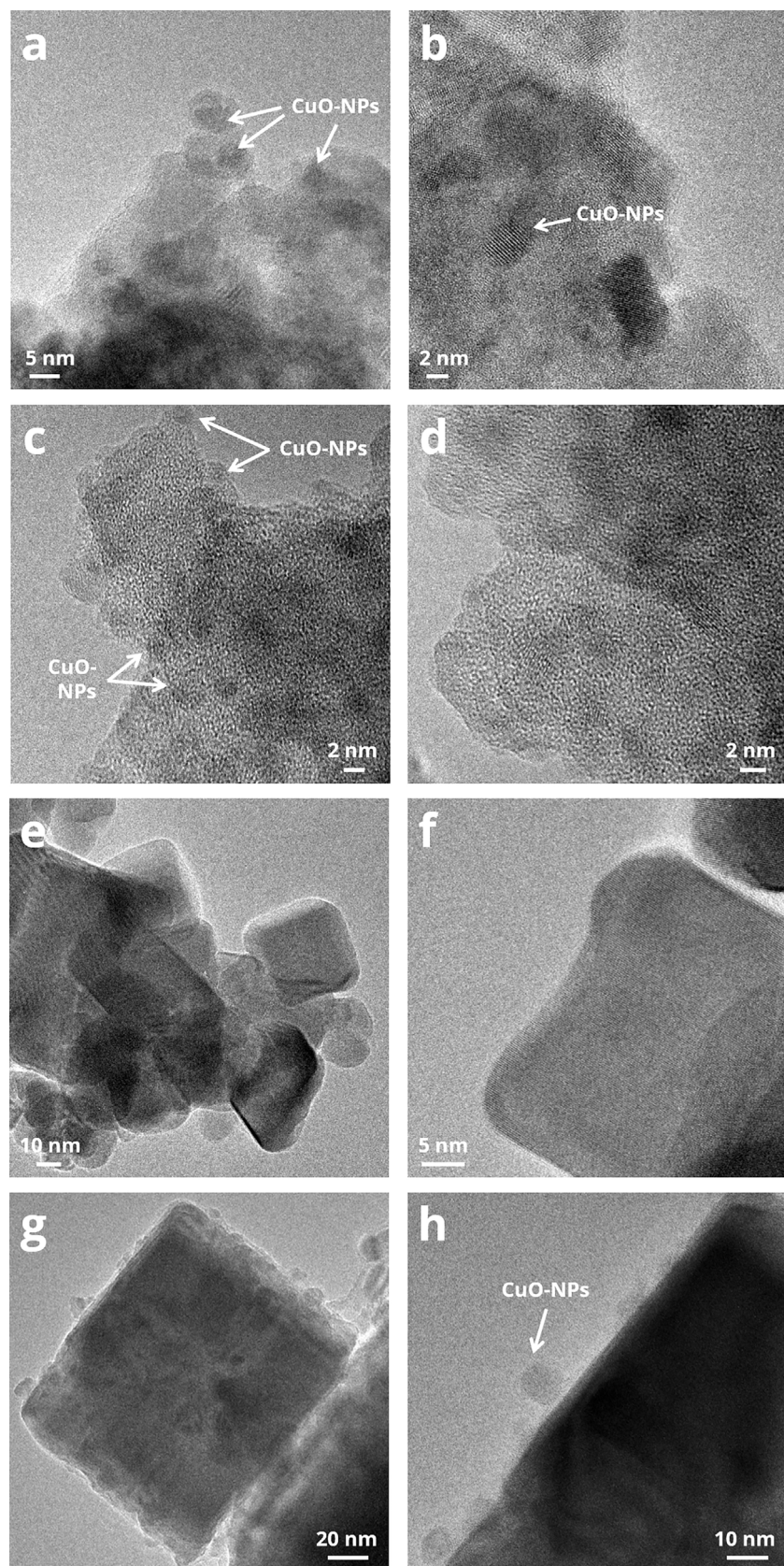


Fig. 3. (A) TEM images of Cu-impregnated catalysts: (a and b) 1% Cu/CeO₂-SCS, (c and d) 5% Cu/CeO₂-SCS, (e and f) 1% Cu/CeO₂-NC and (g and h) 5% Cu/CeO₂-NC. (B) Additional TEM images of Cu-impregnated catalysts: (a) 1% Cu/CeO₂-SCS, (b) 5% Cu/CeO₂-SCS, (c) 1% Cu/CeO₂-NC and (d) 5% Cu/CeO₂-NC. (Bottom) EDX punctual analysis of a STEM-HAADF image of 5% Cu/CeO₂-NC.

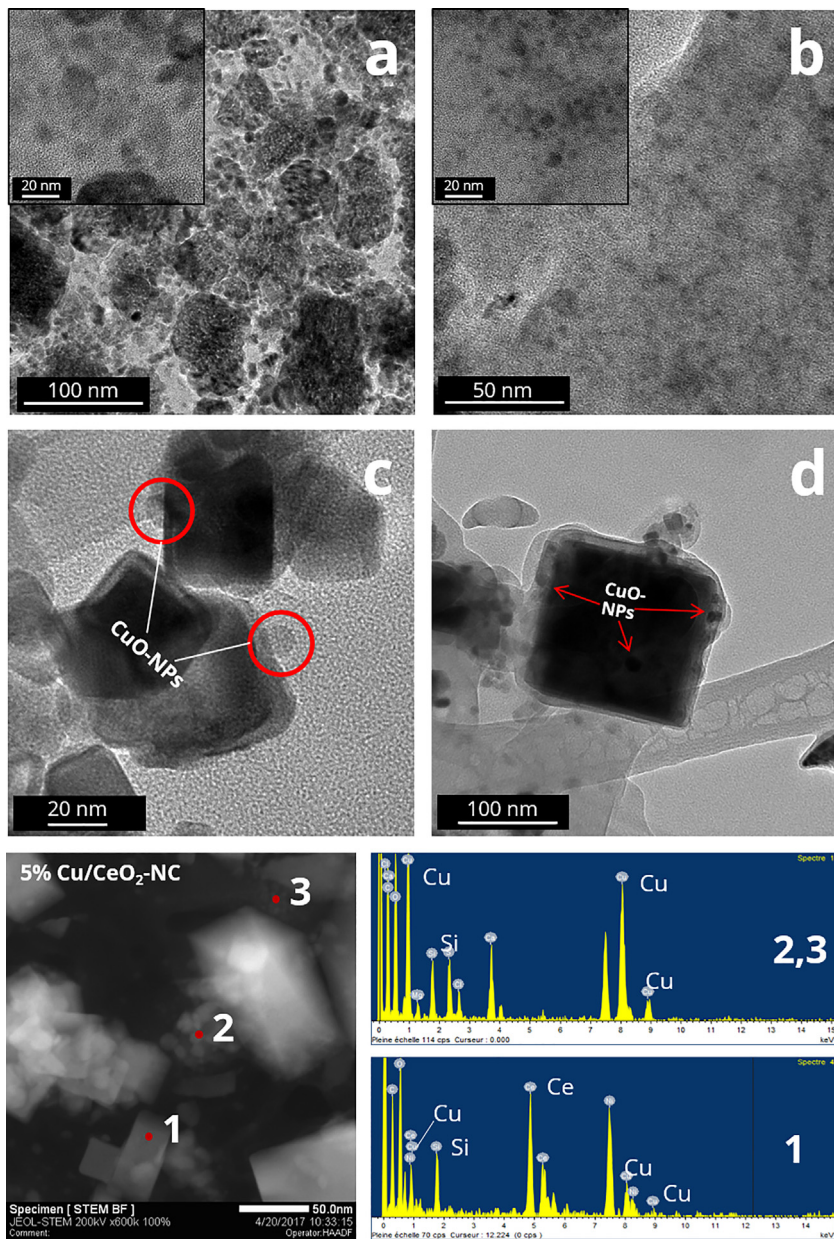


Fig. 3. (A) (Continued)

micrographs (c) and (d)], thanks to the high Cu quantity. The images demonstrate that CuO-NPs are well distributed on the surface. The particle size varies from 2 to 4 nm, similar to the dimension range of colloidal Cu-NPs. On the other TEM images [Fig. 3B, micrograph (b)], the average size of CuO-NPs is around 5 nm, slightly larger than the first area on Fig. 3A. The micrographs (e) and (f) on Fig. 3A show the images of 1% Cu/CeO₂-NC. Unlike on the SC-synthesized samples, on the nanocubic samples the CuO decoration is hardly observed. The surface of a nanocube appears clean and intact. The micrograph (c) on Fig. 3B shows another TEM image of this sample at much higher magnification. Due to the low metal loading, the observation of CuO-NPs was very difficult. Nevertheless, two possible spherical particles with the size of 7–8 nm on the surface of a nanocube may be assigned to CuO-NPs. The micrographs (g) and (h) on Fig. 3A finally shows the images of the 5% Cu/CeO₂-NC sample. Likewise, on the surface of a selected nanocube CuO-NPs are barely observed. Interestingly, the surface appears rougher than that in 1% Cu/CeO₂-NC. On the micrograph (h), clusters attributed to CuO-NPs

are found to decorate a surface of a large nanocube. The size of the pointed particle on the figure is around 7–8 nm. On another TEM image at low magnification [Fig. 3B, micrograph (d)], CuO-NPs are again observed on the surface of a large nanocube but rather with a larger size (8–10 nm). Other CuO-NPs also appear segregated outside the nanocube. This suggests that nanocubic ceria with a very low surface area cannot accommodate well CuO-NPs on the surface.

Results from element mapping via EDX analysis are shown on Fig. 4. Four elements were mapped during the analysis: Ce, Cu, Si and O. Fig. 4a and b show the maps of 1% Cu/CeO₂-SCS and 5% Cu/CeO₂-SCS, respectively. As expected, the invariability in Cu distribution is observed on the surface of both catalysts. The quantity of O and Si also appear homogeneously on the surfaces of interest. Fig. 4a and d show the maps of 1% Cu/CeO₂-NC and 5% Cu/CeO₂-NC. This suggests the homogeneity in Cu distribution on the surface. Additional EDX punctual analysis on an image of 5% Cu/CeO₂-NC under STEM-HAADF mode (Fig. 3B, bottom) shows the presence of Cu on a surface of a nanocube (Point 1). However, the analysis of

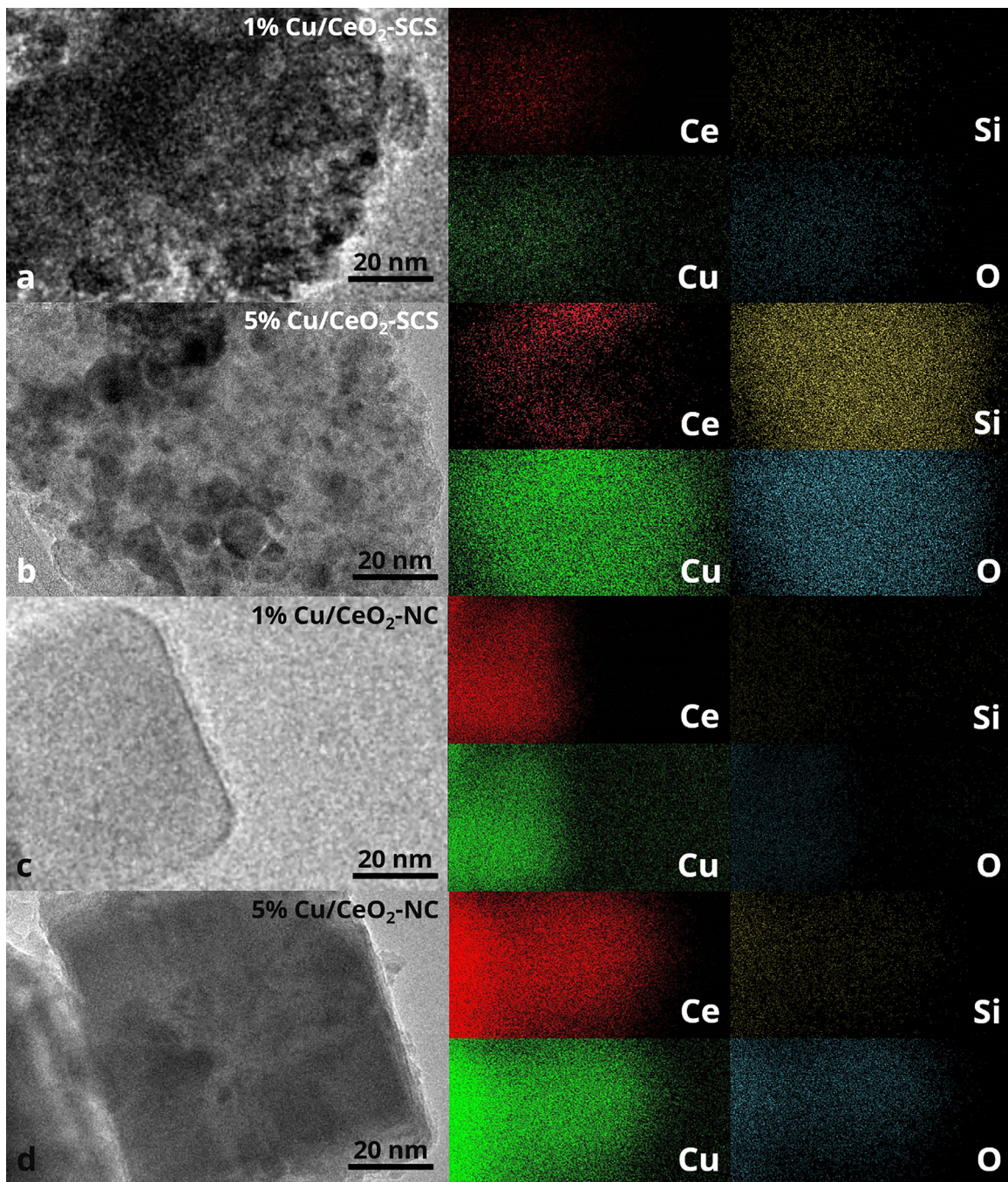


Fig. 4. Element mapping results from EDX of (A) 1% Cu/CeO₂-SCS, (B) 5% Cu/CeO₂-SCS, (C) 1% Cu/CeO₂-NC and (D) 5% Cu/CeO₂-NC.

two different points on somewhat spherical particles (Point 2 and 3) demonstrates the segregation of bulk CuO-NPs outside a nanocube, as the spectra of these two points show a remarkable intensity of Cu (no Ce signal was detected).

3.2. Redox properties and reducibility of the catalysts

Fig. 5A shows the O 1 s XP spectra of all catalysts. In general, high intensity peaks in the binding energy (BE) range of 528.9–529.5 eV that appears in all spectra refer to the typical O²⁻ species originating from metal oxides on the lattice/bulk level [60,61], denoted herein as “O-β”. The secondary peak appearing in higher BE range (530.8–532.3 eV) can be ascribed to chemisorbed oxygen species, such as OH⁻, CO₃²⁻ and O⁻ [62–64], and denoted herein as “O-α”.

Individual assignment of the peaks to these species is rather difficult since high diversity of O-α species by nature results oftentimes in various peak positions at similar BE. Nevertheless, the presence of carbonate species can be estimated via C 1 s XP spectra shown on **Fig. 5C**. The third peak at ca. 288.5 eV can be ascribed to O-C=O species, which is directly linked to carbonate species. In the case of pure ceria samples [spectra (e) and (f)], the intensity of carbonate peak seems higher in the spectra of CeO₂-NC sample than that in the spectra of CeO₂-SCS. High basicity used in the hydrothermal synthesis most likely attracts CO₂ to adsorb on the surface of nanocubes in the form of carbonates. From the O 1 s spectra (**Fig. 5B**), it is noticeable that the peak area of O-α is smaller in the spectra of CeO₂-SCS than that in the spectra of CeO₂-NC. The relative abundance of O-α with respect to O-β, as summarized on **Table 2**, is

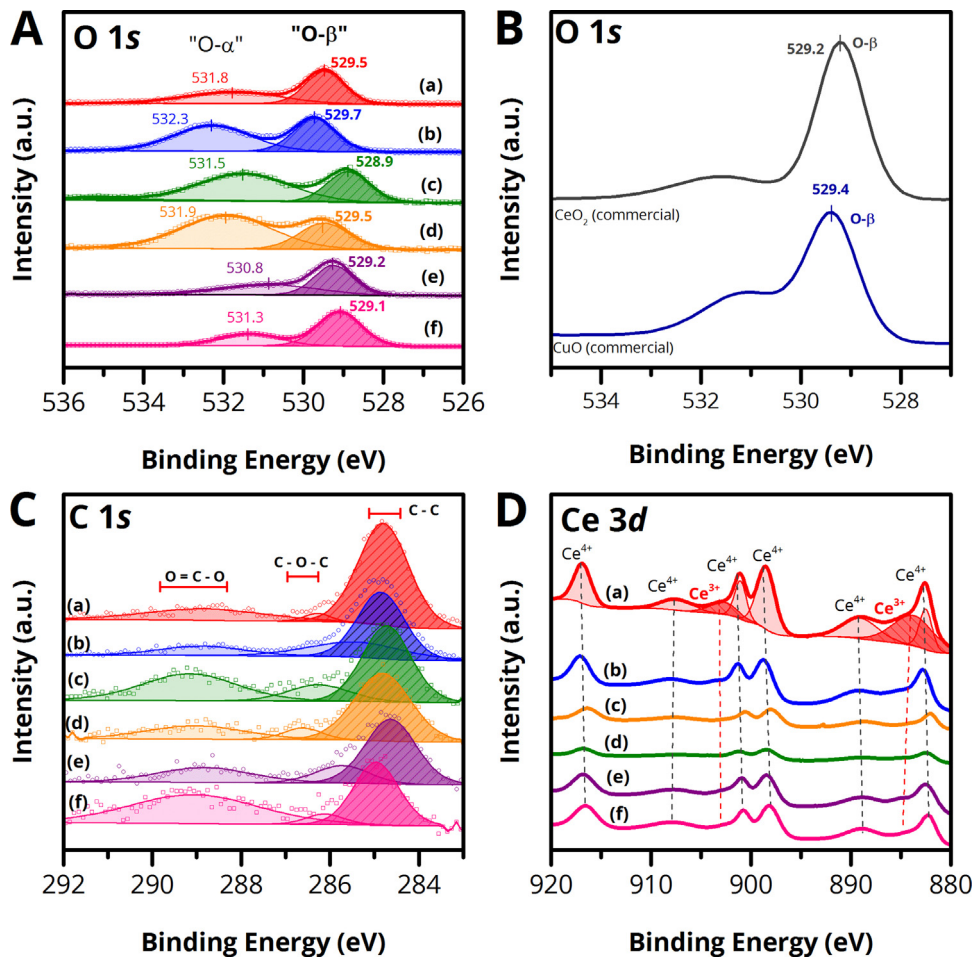


Fig. 5. Deconvoluted XP spectra in the (A) O 1s core level of the prepared catalysts, (B) O 1s core level of the commercial CeO₂ and CuO, (C) C 1s and (D) Ce 3d core levels of the prepared catalysts. List of the prepared catalysts: (a) 1% Cu/CeO₂-SCS, (b) 5% Cu/CeO₂-SCS, (c) 1% Cu/CeO₂-NC, (d) 5% Cu/CeO₂-NC, (e) CeO₂-SCS and (f) CeO₂-NC.

Table 2

Relative abundances of oxygen species derived from deconvoluted O 1s XP spectra.

Sample	O-β		O-α	
	BE (eV)	%-atomic	BE (eV)	%-atomic
1% Cu/CeO ₂ -SCS	529.5	54	530.4	46
5% Cu/CeO ₂ -SCS	529.7	42	530.1	58
1% Cu/CeO ₂ -NC	528.9	33	529.9	67
5% Cu/CeO ₂ -NC	529.5	30	530.4	70
CeO ₂ -SCS	529.3	56	530.8	44
CeO ₂ -NC	529.1	69	531.3	31

evidently higher for CeO₂-SCS than that for CeO₂-NC. These findings from C 1s and O 1s spectra suggest that the majority of the O-α species on the surface of CeO₂-NC comes from carbonates group while the surface of CeO₂-SCS has less carbonates but more other O-α species that most likely come from hydroxyls (OH⁻) group. Physical surface defects are known to be the source of OH⁻ species and have been observed previously via microscopy on the surface of CeO₂-SCS. In the case of CuO-containing samples, the variation in O-β peaks is minor; the difference is only in the chemical shift (higher BE for higher Cu content). For comparison, we have also obtained O 1s spectra of commercial CeO₂ and CuO (Sigma-Aldrich) as shown on Fig. 5B. It can be observed that their O-β peaks also appear at very similar BE (529.2–529.4 eV). Therefore, the contributions of O-Ce and O-Cu contributions on lattice level in our CuO/CeO₂ samples remain indistinguishable. The variation in O-α species, on the other hand, is noticeable for CuO-containing catalysts. From

Table 3

Summary of reduced cerium cation (Ce³⁺) concentrations on the surface of the prepared catalysts.

Sample	Ce ³⁺ concentration (%-atomic)
1% Cu/CeO ₂ -SCS	29
5% Cu/CeO ₂ -SCS	30
1% Cu/CeO ₂ -NC	22
5% Cu/CeO ₂ -NC	19
CeO ₂ -SCS	29
CeO ₂ -NC	21

Table 2, it has been reported that the O-α relative abundance and chemical shift increases as the Cu content increases. From the C 1s spectra (Fig. 5C), the intensity of carbonate species remains low on CeO₂-SCS catalysts despite the impregnation and remains high on CeO₂-NC catalysts. However, the increase in Cu content results in lower carbonate intensity.

Ce 3d deconvoluted spectra of all samples are shown on Fig. 5D. Classical eight peaks are generally identified from the Ce 3d spectrum; two of which are ascribed to reduced cerium species Ce³⁺, while the rest is ascribed to Ce⁴⁺ species [65,66]. In the Ce 3d_{5/2} region, first Ce³⁺ peak appears in the binding energy range of 882.8–884.5 eV while in the Ce 3d_{3/2} region, second Ce³⁺ peak appears in the binding energy range of 901.5–903.7 eV. The relative abundances of all cerium cations are reported on Table S1 (Supporting Information), while those of Ce³⁺ ions for all samples are listed on Table 3. CeO₂-SCS has a relatively higher concentration of reduced cerium cation than CeO₂-NC due to the exothermic nature

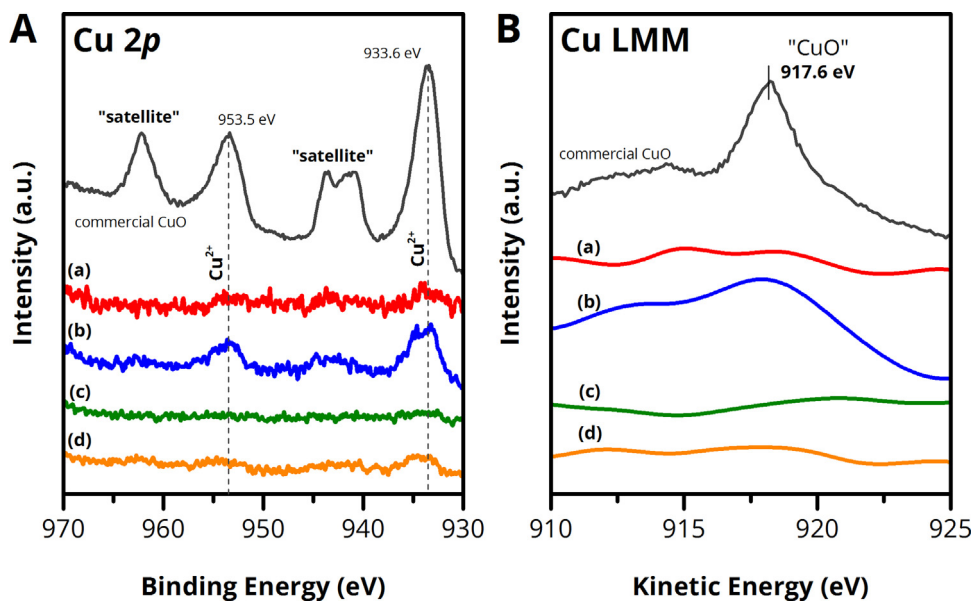


Fig. 6. (A) Cu 2p and (B) Cu LMM Auger XP spectra of a commercial CuO, (a) 1% Cu/CeO₂-SCS, (b) 5% Cu/CeO₂-SCS, (c) 1% Cu/CeO₂-NC and (d) 5% Cu/CeO₂-NC.

Table 4

H₂ uptake ($\mu\text{mol H}_2 \text{ g cat}^{-1}$) and the corresponding peak temperature ($^{\circ}\text{C}$) obtained during H₂-TPR analysis.

Sample	H ₂ uptake ($\mu\text{mol H}_2 \text{ g cat}^{-1}$)			H ₂ /Cu ^d	%-Ce ³⁺ ^e
	200–400 $^{\circ}\text{C}$ ^a	400–500 $^{\circ}\text{C}$ ^b	>500 $^{\circ}\text{C}$ ^c		
1% Cu/CeO ₂ -SCS	921	–	–	921	6.5
5% Cu/CeO ₂ -SCS	1445	–	–	1445	3.1
1% Cu/CeO ₂ -NC	162	38	23	223	1.6
5% Cu/CeO ₂ -NC	176	551	–	727	1.5
CeO ₂ -SCS	–	–	295	295	–
CeO ₂ -NC	–	–	113	113	–

^a Reduction of CuO weakly interacted with ceria on the surface.

^b Reduction of bulk CuO.

^c Reduction of CeO₂.

^d H₂ uptake-to-theoretical Cu quantity ratio; Cu quantity data were taken from Table 1.

^e Percentage of reduced Ce⁴⁺ into Ce³⁺.

of the reaction during the synthesis [40,45]. After the impregnation, regardless of the metal loading, the Ce³⁺ concentration on the surface of CeO₂-SCS remains unchanged (29–30% of Ce³⁺). Similar finding is also observed in the case of CeO₂-NC samples, where the quantity of Ce³⁺ is relatively constant despite the impregnation (19–22%). A minor decrease is somewhat observed from pure CeO₂-NC to 5% Cu/CeO₂-NC.

Fig. 6A shows Cu 2p spectra of all Cu-containing samples and commercial CuO sample (topmost spectrum in grey color). The commercial CuO sample exhibits a typical CuO spectrum; two strong peaks at 933.6 eV and 953.5 eV and their accompanying satellite peaks. Spectra (a) and (c) refer to samples with 1%-wt of Cu loading while spectra (b) and (d) refer to those with 5%-wt of Cu loading. The spectra of low copper content samples seem to have nearly unidentifiable peaks, while those of 5% Cu samples exhibit more pronounced peaks at certain BE ranges. 5% Cu/CeO₂-SCS possesses the clearest spectrum in the series (spectrum (b) in blue), from which one peak is observed at BE range of 933–935 eV in Cu 2p_{1/2} region and another one at the range of 952–954 eV in Cu 2p_{3/2} region. Small shakeups/satellites appear slightly after the main peaks. This spectrum is very similar to CuO as the shakeup peaks, which are the distinctive feature of CuO that never exists in the spectra of other Cu species, are present alongside their major peaks [18,67]. 5% Cu/CeO₂-NC (spectrum (d) in orange) has a much weaker signal intensity than its SCS counterpart. Even so, the typical CuO peaks are still observable. This suggests that the surface

exposed during the analysis most likely contains less Cu content than expected.

The spectra of other Cu species like Cu⁺ or Cu⁰ (metallic) are unfortunately difficult to be deconvoluted in Cu 2p core level, since their peaks overlap at a BE close to that of the major peaks of Cu²⁺ species. To have a better discernment, Cu LMM Auger spectra of the samples are instead analyzed. A typical Cu LMM spectrum has only one major peak at one of these possible three kinetic energies: 918.6, 917.7 and 916.8 eV; each peak position refers to the presence of Cu⁰, Cu²⁺ and Cu⁺ species, respectively [18,68]. Fig. 6B shows the Cu LMM Auger spectra of all Cu-containing samples and the commercial CuO sample. The spectrum of commercial CuO demonstrates one strong peak at KE of 916.7 eV, typical for Cu²⁺ species. The peak of 5% Cu/CeO₂-SCS (spectrum (b) in blue) is the most pronounced among the series and appears at similar value of KE of CuO, hence the assignment of Cu species to Cu²⁺. The presence of Cu⁰ is rather unlikely as no suspicious shoulder peak is observed at KE = 918.6 eV and higher. Other spectra are unfortunately too difficult to analyze as their signals are rather flat with many dubious peaks. However, 5% Cu/CeO₂-NC (spectrum (d) in orange) demonstrates a peculiarly similar spectrum to the one of 5% Cu/CeO₂-SCS. This might also imply the dominance of CuO in the sample.

Fig. 7 shows the H₂-TPR profiles of the prepared catalysts. Fig. 7A shows the profiles of the SC-synthesized catalysts while Fig. 7B shows the profiles of the nanocubic catalysts. The profiles of pure ceria samples (purple curve on Fig. 7A = CeO₂-SCS, pink

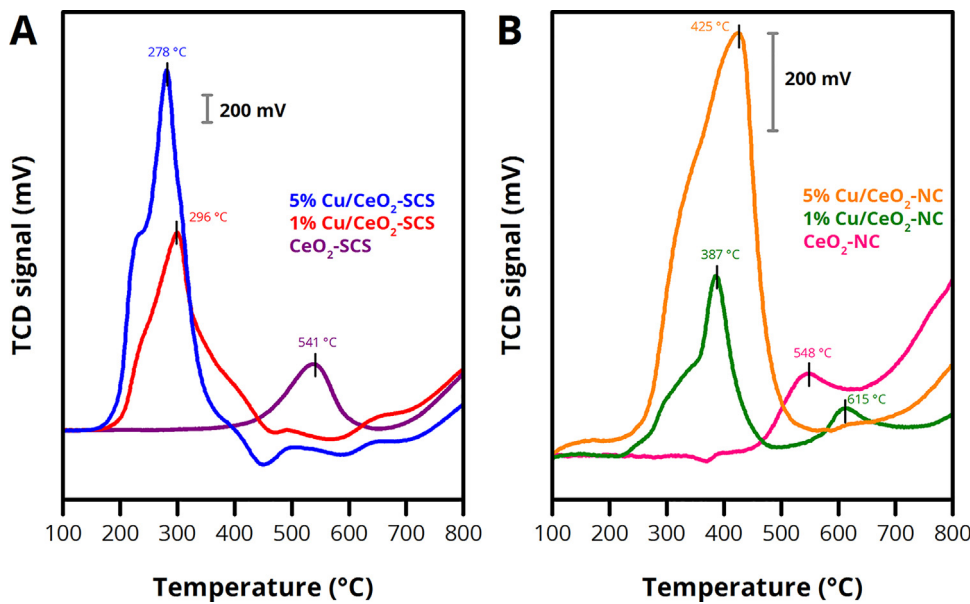


Fig. 7. H_2 -TPR profiles of (A) SC-synthesized and (B) nanocubic catalysts.

curve on Fig. 7B = CeO_2 -NC) exhibit typical H_2 -TPR trend of pure ceria: one reduction peak at high temperature (541°C and 548°C for CeO_2 -SCS and CeO_2 -NC respectively) and a continuous catalyst reduction above 600°C [40,43,46,69]. Table 4 summarizes the H_2 uptake (in $\mu\text{mol H}_2 \text{ g cat}^{-1}$) of the prepared catalysts, categorized per peak temperature, the total H_2 uptake-to-theoretical Cu quantity ratio (denoted as H_2/Cu) and the percentage of Ce^{4+} species reduced into Ce^{3+} (denoted as %- Ce^{3+}). It appears that the H_2 uptake on CeO_2 -SCS is higher than CeO_2 -NC, most likely due to higher catalyst surface area. The reduction peaks on the profile of Cu-containing catalysts fall in a lower temperature range, in which we discern two kinds of CuO reduction: (1) reduction of CuO species weakly interacted with ceria on the surface at 200 – 400°C , and (2) reduction of bulk CuO at 400 – 500°C . The Cu/CeO_2 -SCS samples enable a large H_2 uptake (921 and $1445 \mu\text{mol H}_2 \text{ g cat}^{-1}$ for 1% Cu/CeO_2 -SCS and 5% Cu/CeO_2 -SCS, respectively), that entirely occurs at the first temperature range. Meanwhile, the H_2 uptake on the Cu/CeO_2 -NC samples occur at both temperature ranges and the total values are much lower than those of the Cu/CeO_2 -SCS samples (223 and $727 \mu\text{mol H}_2 \text{ g cat}^{-1}$ for 1% Cu/CeO_2 -NC and 5% Cu/CeO_2 -NC, respectively). 5% Cu/CeO_2 -NC, in particular, exhibits a large reduction peak at 400 – 500°C (H_2 uptake at about $551 \mu\text{mol H}_2 \text{ g cat}^{-1}$), thus suggesting the presence of bulk CuO possibly segregated from ceria surface. The H_2/Cu ratios for Cu/CeO_2 catalysts are generally higher than 1 , meaning that reduction at low temperature not only occurs on CuO but also on ceria, most likely due to ceria polarization by interaction with vicinal Cu atoms [48]. The ratios for Cu/CeO_2 -SCS catalysts are significantly higher than those for Cu/CeO_2 -NC catalysts, hence implying stronger $\text{Cu} - \text{O} - \text{Ce}$ interaction on the surface of CeO_2 -SCS than that of CeO_2 -NC. The estimated percentage of Ce^{4+} species reduced into Ce^{3+} , assuming that all Cu^{2+} species are reduced into Cu^0 , generally increases as the copper content of the sample increases, irrespective of the morphology. The values of %- Ce^{3+} are the highest for the Cu/CeO_2 -SCS samples, suggesting the stronger reducing effect of CuO on ceria.

3.3. Catalytic activities

3.3.1. CO oxidation

Fig. 8 shows CO conversions over all the prepared catalysts as a function of temperature. In the case of pure ceria samples, CeO_2 -

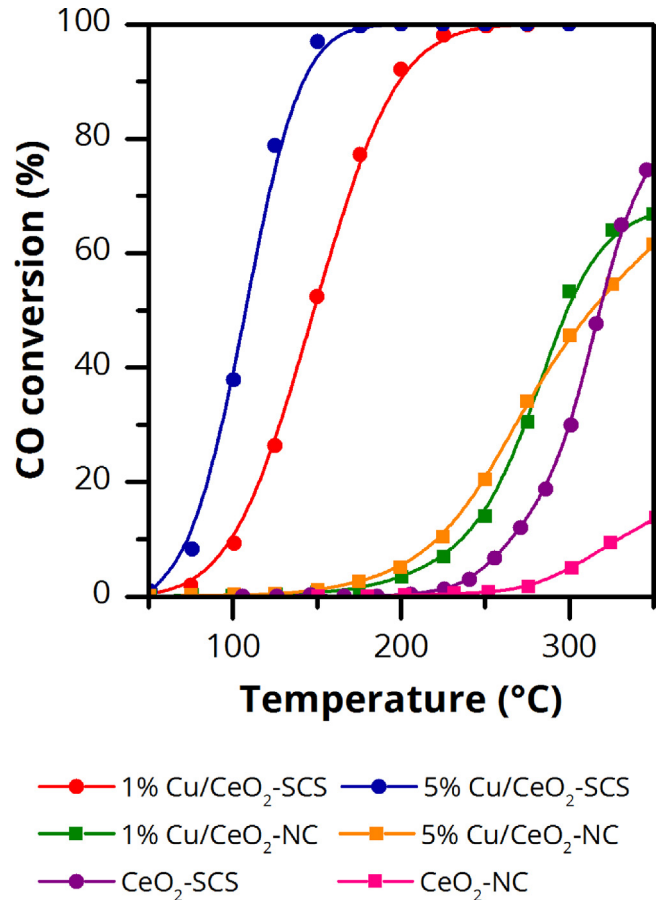


Fig. 8. CO conversion as a function of temperature over all catalysts.

NC appears less active towards CO oxidation than CeO_2 -SCS. The trend is somewhat dissimilar from what has been reported elsewhere [43,46], due to variability in synthesis parameters. As seen on the figure, low-temperature high CO conversion is attainable with Cu-containing catalysts, irrespective of the metal loading. The presence of CuO clusters clearly enhances the catalytic activities of

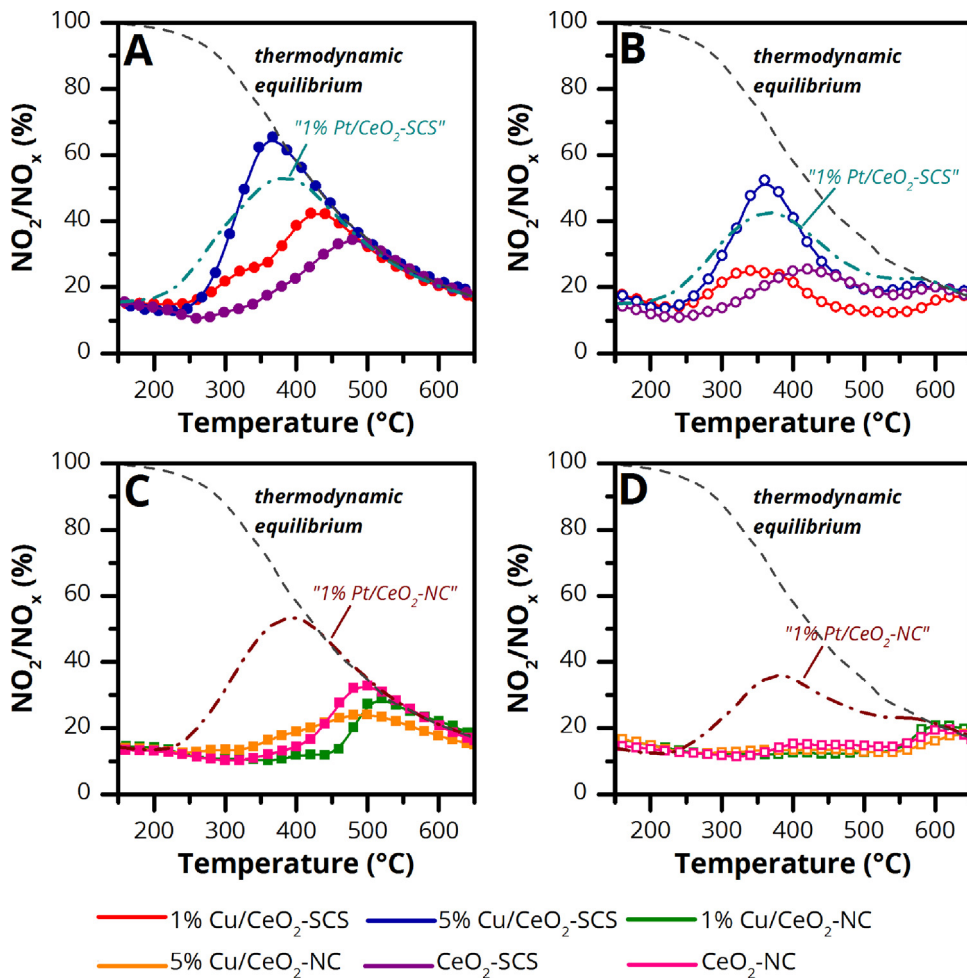


Fig. 9. NO₂ molar percentage as a function of temperature obtained from catalytic tests with SC-synthesized and nanocubic catalysts in the absence of soot (A and C) and in the presence of soot (B and D).

pure ceria by lowering the reaction temperature; the difference of which can even reach up to 200 °C in the case of the CeO₂-SCS samples. The SC-synthesized catalysts generally perform better than their nanocubic counterparts. 5% Cu/CeO₂-SCS (blue curve) is particularly the most active catalyst among the series. Surface area of the support might initially be the reason for the high catalytic performances of the CeO₂-SCS catalysts. It has also been known from H₂-TPR analysis (*vide supra*) that the impregnated CuO-NPs on the surface of CeO₂-SCS are present abundantly as the species weakly interacted with ceria on the surface via Cu – O – Ce bond. This gives rise to an easier reducibility of ceria on the surface and, furthermore, to an enhanced oxygen intake on ceria (due to more vacancies). Such properties can be beneficial for CO oxidation as several mechanisms, such as Langmuir-Hinshelwood (L-H) and Mars-van Krevelen (M-vK), necessitate an oxygen mobility on ceria surface. The former mechanism (L-H) appears to be predominant in governing CO oxidation over our Cu/CeO₂-SCS catalysts since small CuO clusters on the surface of ceria (as seen on the previous TEM images) can be the active sites for CO oxidation. By default, the L-H mechanism starts with non-dissociative adsorption of CO and dissociative adsorption of O₂ (into two O adatoms), then proceeds with the reaction between CO and O adatom on the surface of CuO and finally ends with CO₂ desorption. Thanks to the Cu – O – Ce interaction on the surface, the O adatom can spillover from copper phase to ceria surface (filling in the oxygen vacancy near the inter-

face) and can actively attack adsorbed CO molecule forming CO₂, hence more efficient oxidation.

Our nanocubic samples, on the other hand, have demonstrated lower CO oxidation performances. The increase of Cu content does not seem to significantly affect the catalytic activity. From the H₂-TPR results, it has been known that the reducibility of Cu/CeO₂-NC catalysts is much lower than that of Cu/CeO₂-SCS. It has also been observed that the reduction over CuO/CeO₂-NC catalysts takes place at a relatively higher temperature than that of CeO₂-SCS catalysts, thus suggesting the presence of CuO bulk. This has been confirmed via TEM images and EDX analysis, which have shown the segregation of CuO clusters outside the nanocubes. Bulk CuO (tenorite) has been proven in the literature inactive towards CO oxidation and high loading of it can lower the catalytic activity due to the coverage of active surface of the catalyst [48,50,67,70].

3.3.2. NO oxidation

Fig. 9 shows profiles of NO₂ percentage in NO_x mixture (NO + NO₂) during NO oxidation catalytic tests as functions of temperature. Fig. 9A and C refer to the results from the catalytic tests in the absence of soot, while Fig. 9B and D summarize the results from NO_x-assisted soot oxidation catalytic tests. The latter figures will be discussed in Section 3.3.4. On Fig. 9A, it is evident that the SC-synthesized catalysts have higher NO conversions than their nanocubic counterparts (Fig. 9C). 5% Cu/CeO₂-SCS (blue curve), in particular, gives the broadest reaction temperature window, the

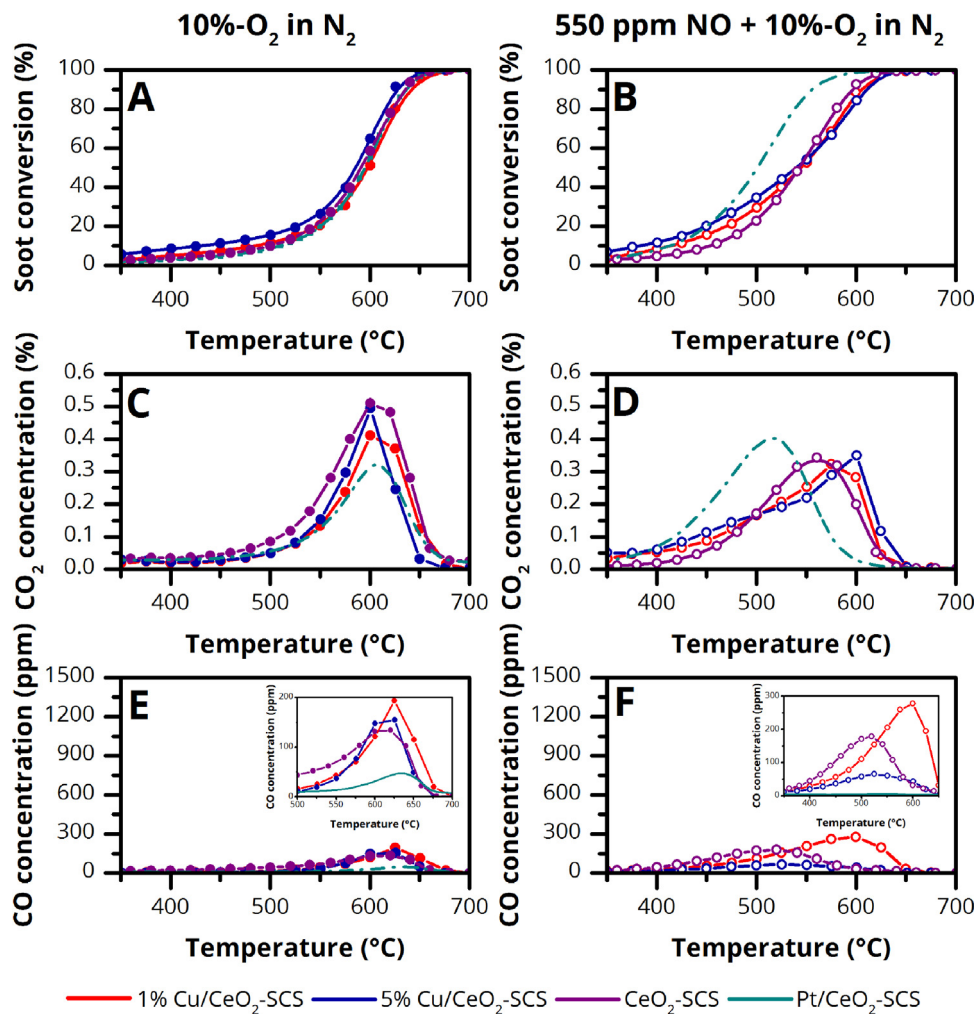


Fig. 10. Soot conversion, CO_2 and CO concentrations over Cu/CeO_2 -SCS catalysts as a function of temperature obtained from catalytic tests in the absence of NO_x (A, C and E) and in the presence of NO_x (B, D and F).

earliest light-off and the highest peak NO_2 percentage (about 60 percent). We compare this catalyst with our Pt-catalyst (1%-wt of Pt) in the previous work (denoted on the figure as “ Pt/CeO_2 -NC” and “ Pt/CeO_2 -SCS”) in terms of NO_2 percentage [33] and we discover that the activity of 5% Cu/CeO_2 -SCS is higher. Lower Cu content evidently gives lower NO conversion, as can be seen from the peak of the profile of 1% Cu/CeO_2 -SCS (red curve), at higher temperature. Based on this observation, we suggest that with the SC-synthesized support the increase in Cu quantity impacts positively on the catalytic activity. According to the literature, catalyzed NO oxidation conforms to Langmuir-Hinshelwood (L-H) mechanism [71,72], where metal active sites must have small particle size and be well-dispersed on the surface of the support. Our characterization data have shown that CuO -NPs are evenly distributed on CeO_2 -SCS surface and their small dimension is still retained. Moreover, the easier reducibility of these samples can give rise to more enhanced oxygen vacancies near ceria-copper interface, thus enabling oxygen spillover from copper to ceria surface.

As seen on Fig. 9C, NO oxidation over pure CeO_2 -NC catalyst (pink curve) lights off at ca. 400 °C and reaches its peak NO_2 production at about 500 °C. A different trend, however, is observed in the Cu-containing catalysts. 1% Cu/CeO_2 -NC shows a small peak of NO_2 at about 520 °C, evidently higher than that of CeO_2 -NC. The peak also appears lower in intensity. NO oxidation over 1% Cu/CeO_2 -NC lights off later than CeO_2 -NC; the temperature differ-

ence is about 50 °C. Surprisingly, the activity of 5% Cu/CeO_2 -NC is the lowest among the series. The NO_2 production peak is very broad but unfortunately low in intensity. The peak temperature is slightly lower than that of CeO_2 -NC. However, the reaction over this catalyst lights off much earlier than the other two in the series at ca. 350 °C. These results suggest that the increase in Cu quantity and/or the lower metal dispersion due to larger NPs on the surface of nanocubic ceria gives an adverse impact on the catalytic activity. This could be due to the presence of bulk CuO , as understood from H_2 -TPR and TEM images, that may be inactive towards NO oxidation.

3.3.3. NO_x -free soot oxidation

Figs. 10 and 11 show the profiles of soot conversion, CO and CO_2 concentrations during the soot oxidation catalytic tests over SCS-based and nanocubic catalysts, respectively, in the absence of NO (first column, left) and in the presence of NO (second column, right). In this section, will be discussed only the catalytic activity towards NO_x -free soot oxidation. Several important numbers concerning the catalytic activities are summarized on Table 5. The classical parameter, $T_{\text{conversion}(\%)}$, refers simply to the temperature at which soot is burnt at given conversion.

In general, the performances of Cu/CeO_2 -NC catalysts are higher than those of Cu/CeO_2 -SCS catalysts. 1% Cu/CeO_2 -NC (green curve on Fig. 11A), particularly, leads in the performance, surpassing 5% Cu/CeO_2 -SCS (blue curve on Fig. 10A). The $T_{50\%}$ is about 552 °C

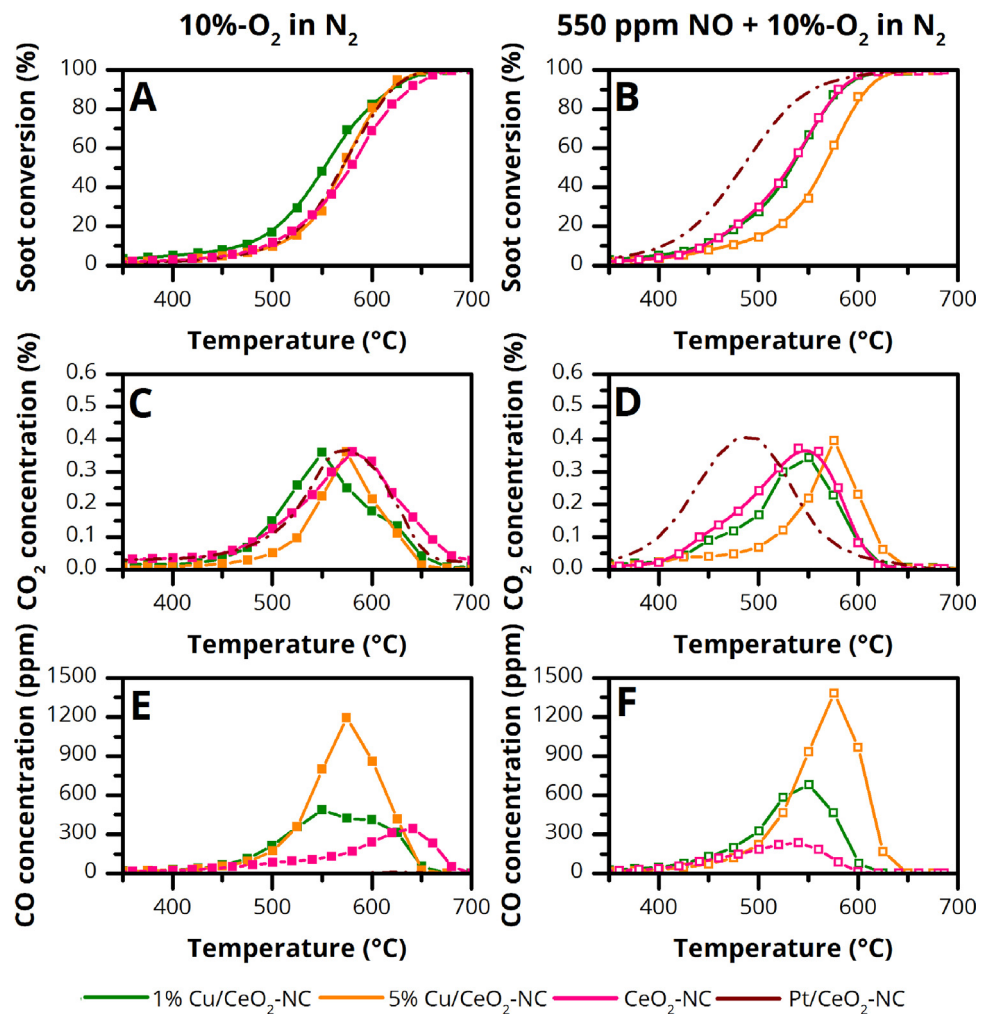


Fig. 11. Soot conversion, CO_2 and CO concentrations over Cu/CeO_2 -NC catalysts as a function of temperature obtained from catalytic tests in the absence of NO_x (A, C and E) and in the presence of NO_x (B, D and F).

Table 5

Results from soot oxidation catalytic tests in the absence and the presence of NO_x (fresh catalysts).

In the absence of NO_x (10% v O_2 in N_2)			
Sample	$T_{10\%}$ (°C)	$T_{50\%}$ (°C)	$T_{90\%}$ (°C)
1% Cu/CeO_2 -SCS	484	599	638
5% Cu/CeO_2 -SCS	441	588	624
1% Cu/CeO_2 -NC	475	552	617
5% Cu/CeO_2 -NC	504	571	615
CeO_2 SCS	502	591	635
CeO_2 NC	492	580	637
In the presence of NO_x (550 ppmv $\text{NO} + 10\%$ v O_2 in N_2)			
Sample	$T_{10\%}$ (°C)	$T_{50\%}$ (°C)	$T_{90\%}$ (°C)
1% Cu/CeO_2 -SCS	415	545	603
5% Cu/CeO_2 -SCS	384	540	608
1% Cu/CeO_2 -NC	444	534	579
5% Cu/CeO_2 -NC	472	567	605
CeO_2 -SCS	453	544	596
CeO_2 -NC	446	531	580

and undoubtedly the lowest amongst others. Although the $\text{Ce} 3d$ XP spectra and H_2 -TPR analysis have shown that the Cu/CeO_2 -SCS catalysts have higher quantity of reduced cerium species and reducibility than the Cu/CeO_2 -NC catalysts, the activity of soot oxidation seems to depend more on the catalyst morphology.

The importance of well-defined nanostructure, especially ceria nanocubes, has been emphasized in our recent investigations, as shapes with low-index planes are more reactive towards soot oxidation [33,45,46]. The activity of 1% Cu/CeO_2 -NC is surprisingly higher than that of our most performing Pt/CeO_2 -NC (dark red curve on Fig. 11A), thus suggesting that CuO promotes better oxygen transfer from bulk to ceria-soot interface than Pt. The activity of 5% Cu/CeO_2 -NC (orange curve on Fig. 11A) is, however, lower than 1% Cu/CeO_2 -NC. This suggests that high Cu content on nanocubic ceria also gives an adverse effect on soot oxidation catalytic activity. High reaction selectivity to CO_2 is evidently confirmed for the SC-synthesized catalysts as the CO concentrations are very low (observed on Fig. 10E) and balanced with high CO_2 concentrations (observed on Fig. 10C). In contrast, CO concentrations are markedly high in the case of nanocubic catalysts. The increase in Cu content contributes rather proportionally to the increase in CO production, and consequently the decrease in CO_2 selectivity. This phenomenon is simply linked to the activity of the catalysts towards CO oxidation, which is clearly higher over the SC-synthesized catalysts than over the nanocubic ones.

3.3.4. NO_x -assisted soot oxidation

Figs. 10 B and 11 B show the soot conversion as a function of temperature over SCS-based and nanocubic catalysts, respectively, during the tests with NO_x -assisted soot oxidation. 5% Cu/CeO_2 -

SCS (blue curve on Fig. 10B) shows an exceptionally high catalytic activity between 300 and 500 °C and is followed by 1% Cu/CeO₂-SCS that is less active. However, these catalysts are surpassed by the nanocubic samples at high temperature reaction, starting from 500 °C. From Fig. 11B, it appears that both CeO₂-NC (pink curve) and 1% Cu/CeO₂-NC have similar activities, as the two curves appear to superpose each other. The activity of 5% Cu/CeO₂-NC, as expected, is the lowest in the series and even among all catalysts.

High activity at low temperature over the series of SC-synthesized catalysts confirms the role of NO₂ in initiating soot oxidation, that is the takeover of oxidant role from the oxygen. The oxidation with oxygen, uncatalyzed or catalyzed, is impossible to occur at low temperature. NO₂, once formed in the reactor, reacts instantly with soot and even more quickly at higher temperature. This uniquely takes place over the SC-synthesized catalysts, as NO oxidation over these materials lights off early (see Section 3.3.2). We suggest that within the temperature range of 250–400 °C the reaction is highly controlled by the presence of NO₂. This also explains the low catalytic activity over the nanocubic catalysts within the temperature range aforementioned since NO conversion to NO₂ remains impossible. Above 500 °C, nanocubic catalysts (excluding 5% Cu/CeO₂-NC) appear more active than the SC-synthesized ones. We surmise that this is due to the effect of support morphology and that the role of oxidant is shared between NO₂ and O₂. However, since the quantity of bulk oxygen is much higher than that of NO₂, the reaction is dominated by the normal soot oxidation, in which the nanocubic catalysts are more active than the SC-synthesized ones.

Fig. 9B and D show the profiles of NO₂ percentage in NO_x mixture (NO + NO₂) during NO oxidation catalytic tests in the presence of soot as a function of temperature. Using Fig. 9A and C as the reference, it is well understood that in the presence of soot NO₂ production becomes low. In the case of 5% Cu/CeO₂-SCS (blue curve), the oxidation reaction in the presence of soot lights off at a similar temperature to that in the absence of soot. Upon heating, the NO₂ production increases but this time less sharply, as seen from the increasing trend after 250 °C. This signifies the early consumption of NO₂ although it appears quite insignificant. Then, the reaction continues yielding NO₂ till the peak production that is lower than that in the absence of soot and far from the equilibrium, followed eventually by a gradual decrease of NO₂ to its equilibrium concentration at high temperature (see Fig. 9B). Based on this trend, we surmise that at 400 °C active participation of NO₂ in the reaction still remains even though oxygen starts dominating. Above 500 °C, the importance of NO₂ is low in the reaction and oxygen starts reacting with soot non-catalytically. Likewise, the trend is observed in other SC-synthesized samples although it may differ in peak temperatures. However, the nanocubic catalysts, as expected, have different NO₂ profiles. Being almost inactive at low temperature, no peaks are observed at low temperature. The curves of all nanocubic catalysts appear constantly flat even at high temperature. The disappearance of NO₂ is observed already at 400 °C in the case of CeO₂-NC and 1% Cu/CeO₂-NC while it occurs earlier at 300 °C in the case of 5% Cu/CeO₂-NC. Even so, the production of NO₂ is initially low compared to that over SC-synthesized catalysts. Therefore, the complete participation of NO₂ does not contribute much to the improvement of overall catalytic activity.

3.4. Stability of the catalysts

In order to assess the stability of CuO-NPs, a series of stability tests has been carried out. Fig. 12 shows the soot conversion profiles obtained from three cycles of NO_x-assisted soot oxidation during the stability test. Fig. 12A, B and C exhibit the profiles during fresh run, first repetition and second repetition, respectively. A distinct difference in activity is observed for 5% Cu/CeO₂-SCS (blue

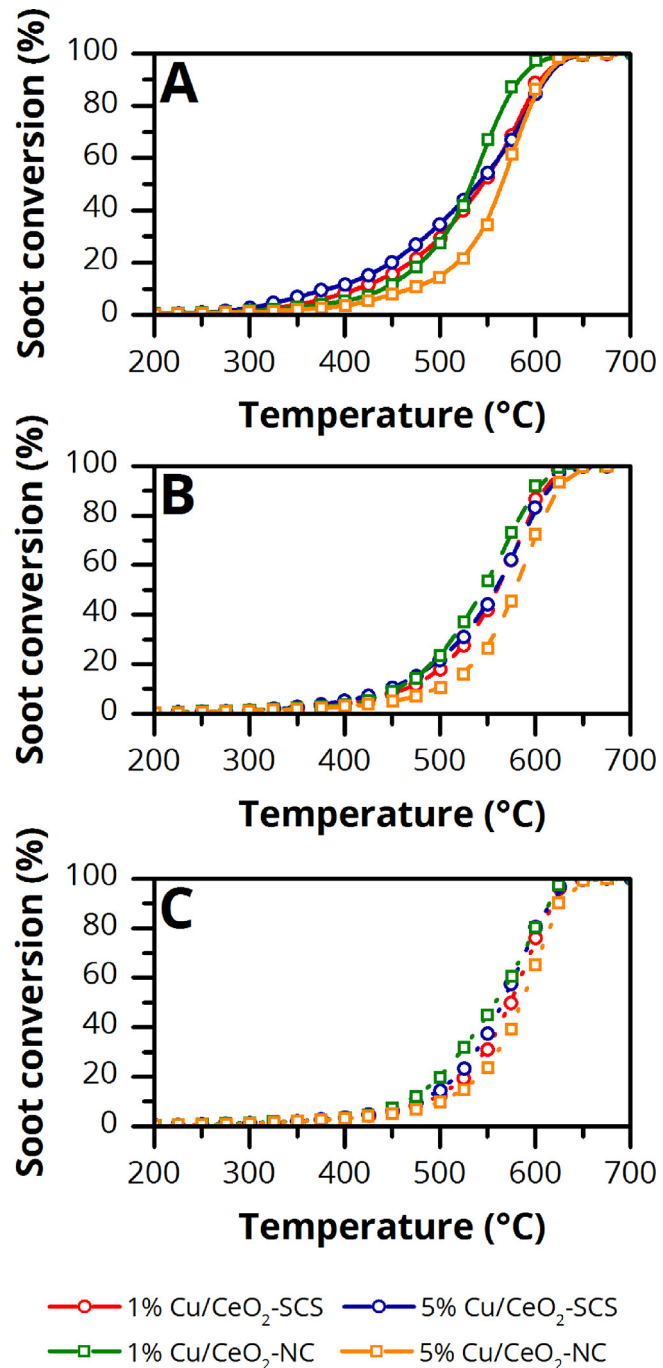


Fig. 12. Soot conversion as a function temperature obtained from stability test: (A) fresh run, (B) first repetition and (C) second repetition.

curve). We pick 450 °C as the temperature of reference (T_{ref}) and we observe that the conversion becomes lower as the number of repetition increases. The fresh 5% Cu/CeO₂-SCS catalyst initially mediated ca. 20% of soot conversion, but then started losing its activity in the first repetition (conversion at ca. 10%) and finally became worse in the second repetition (conversion at ca. 5%). Similar trend is observed on the profiles of other catalysts albeit scarcely. Fig. 13 summarizes the $T_{50\%}$ data of all Cu-containing catalysts during fresh run, first repetition and second repetition. Brief comparison of the data between fresh run and first repetition has demonstrated that the deactivation occurs early after the first repetition, as the temperature difference can reach 20 °C. The activity continues to decline after the second repetition but the decrement

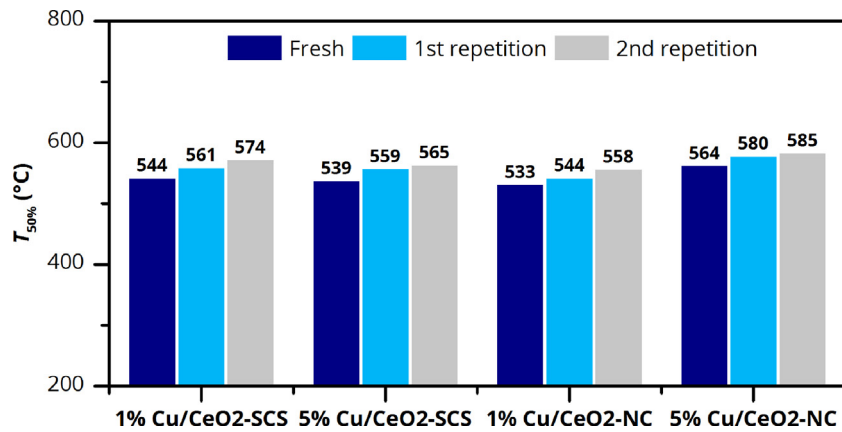


Fig. 13. Summary of $T_{50\%}$ of NO_x -assisted soot oxidation obtained from stability test.

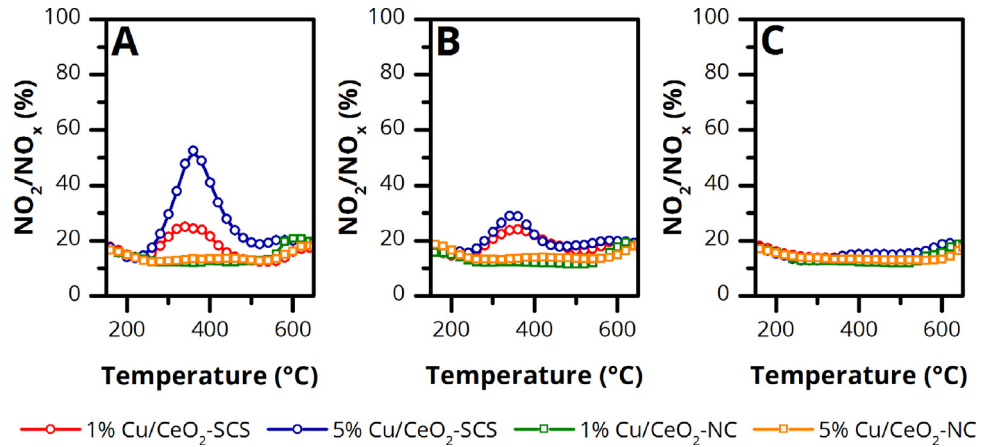


Fig. 14. NO_2 molar percentage as a function of temperature obtained from stability test: (A) fresh run, (B) first repetition and (C) second repetition.

is rather small, especially in the case of nanocubic samples. After being thermally treated up to 700 °C, all catalysts lost their ability to mediate NO oxidation, which is the most important step in the reaction. Since copper mediates the reaction, we suggest that deactivation of copper particles by sintering occurred during the thermal treatment. To reinforce our evidence, we plot also the data of NO_2 percentage during the reaction as a function of temperature on Fig. 14. The most active catalyst in fresh condition, 5% Cu/CeO₂-SCS, has the most visible decrease of activity towards the reaction; the intensity of peak diminishes until no longer NO_2 is produced during the second repetition (Fig. 14C). The activity towards NO oxidation of 1% Cu/CeO₂-SCS is still maintained during the first repetition but is very low during the second repetition. The nanocubic samples have not demonstrated any significant catalytic activities towards NO oxidation from the fresh run. For this reason, the decrease in specific rate between two repetitions appears relatively lower compared to that of the SC-synthesized catalysts.

To better assess the particle sintering phenomenon, we have performed element mapping via EDX of the spent catalysts. Fig. 15 shows four element maps (Ce, Cu, Si and O) on the selected surfaces of the catalysts. The first set of maps (Fig. 15a) belongs to 1% Cu/CeO₂-SCS. The selected zone exhibits uncommon shapes of SC-synthesized ceria; the particles are rather spherical and non-corrugated. The element maps of this zone show that there is almost no Ce detected in the area of interest. Cu evidently predominates while Si and O appear rather scarcely. This suggests that

after three cycles of reaction Cu-NPs uncontrollably migrate, coalesce with each other and eventually undock from the ceria support, forming a segregated phase of CuO_x. While it has been understood that silane-stabilized Pt [33] and Ni nanoparticles [32] can lead to sintering-resistant materials due to the formation of silica patches surrounding the particles during calcination step, a different interaction between Si and Cu in silane-stabilized Cu nanoparticles is more likely to exist. The second set (Fig. 15b) belongs to 5% Cu/CeO₂-SCS. We have selected the zone that is more typical of CeO₂-SCS (spongy, rough surfaces) in order to see better the distribution of Cu on ceria. The element maps show that in this zone both Ce and Cu exist in the area of interest. However, it is observed carefully that Ce concentrates more on the upper left area, marked on the corresponding TEM image by the dark zone, while Cu populates on the lower right area. This finding evidences phase segregation on the surface. Fig. 15c shows the set of element maps of 1% Cu/CeO₂-NC. From the difference of luminosity, it seems that in the area of interest Ce is much less dominant than Cu. Ce concentrates on the big, nanocubic agglomerate but exists in a very low amount on the small, spherical agglomerates (on the TEM image, bottom). This is the same phenomenon observed previously in the element maps of 1% Cu/CeO₂-SCS. Finally, the analysis is closed with the maps of 5% Cu/CeO₂-NC shown on Fig. 15d. The Cu segregation is hardly observed in the area of interest as Ce and Cu seem to coexist in the sample. However, through a very careful observation on the spherical agglomerates (on the TEM image, bottom-right), the equivalent

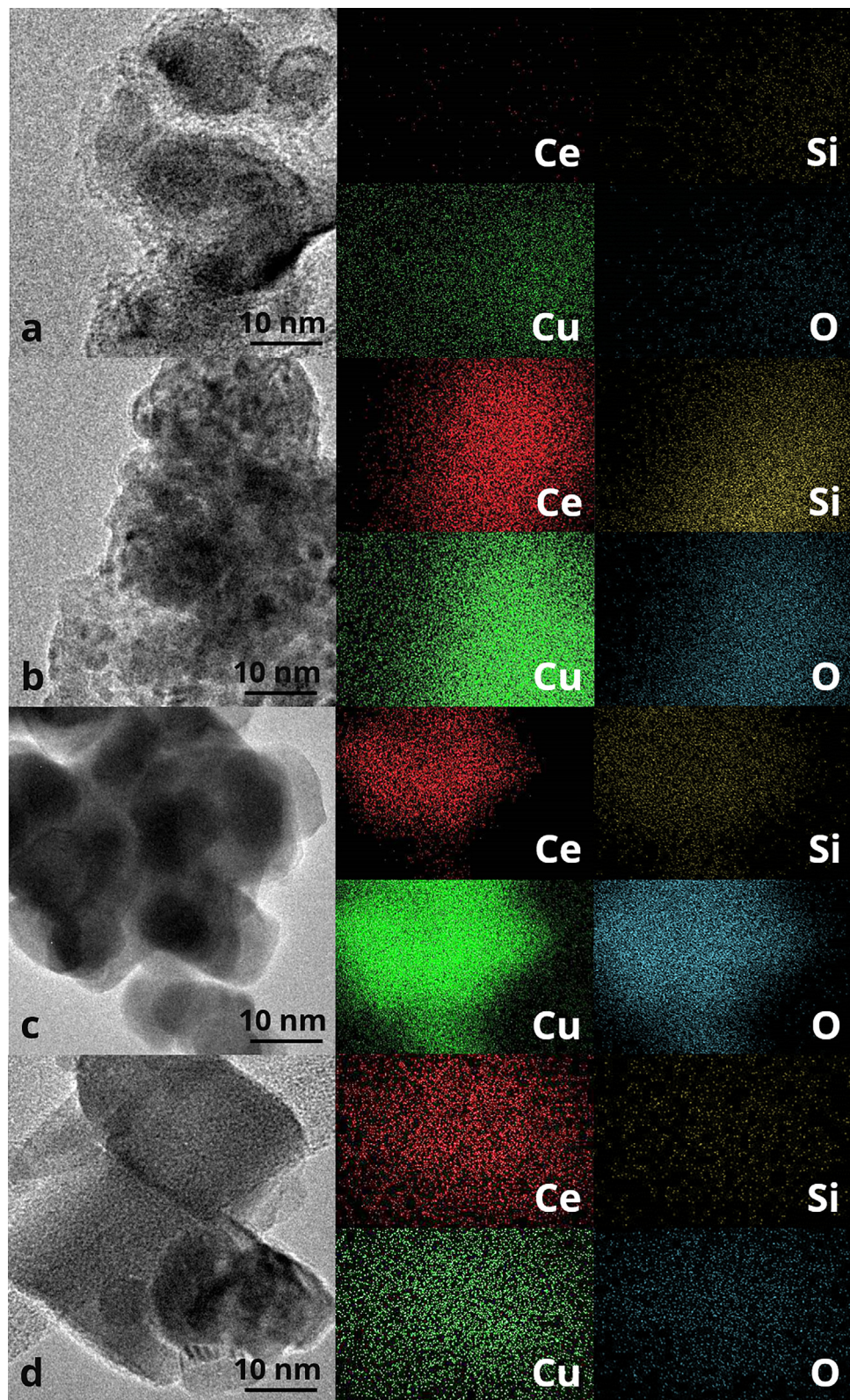


Fig. 15. Element mapping results from EDX of aged catalysts: (A) 1% Cu/CeO₂-SCS, (B) 5% Cu/CeO₂-SCS, (C) 1% Cu/CeO₂-NC and (D) 5% Cu/CeO₂NC.

area in Cu map appears slightly denser than the rest of the sample, while in Ce map the density seems normal.

4. Conclusion

In this work, we have prepared Cu colloids stabilized by organosilane. We have deposited these colloids as copper oxide nanoparticles (CuO-NPs) onto two ceria supports with substantially different morphologies at two different metal loadings. We have assessed the activity of our catalysts towards four different reactions and we finally have come to several conclusions:

- Cu/CeO₂-SCS catalysts give positive effect on CO oxidation and NO oxidation mainly due to their easier reducibility as well as better dispersion on the surface than their nanocubic counterparts. The presence of segregated bulk CuO in Cu/CeO₂-NC catalysts renders the material inactive towards the two reactions.
- In the absence of NO_x, CuO functions better with CeO₂-NC in enhancing soot oxidation since the effect of support morphology towards the reaction predominates. In the presence of NO_x, as one might expect, CuO functions better with CeO₂-SCS as the consequence of better NO oxidation.

We have also assessed the stability of CuO-NPs by testing the catalysts three times with NO_x-assisted soot oxidation and we have discovered that after three cycles CuO-NPs suffer from sintering; the mechanism involves particle migration and coalescence. Future work concerning these materials will be focused on limiting these degradation phenomena.

Appendix A. Supplementary data

Supplementary data associated with this article can be found, in the online version, at <http://dx.doi.org/10.1016/j.apcatb.2017.05.061>.

References

- [1] R. Paranjape, A.K. Suresh, P. Aghalayam, Understanding Pt-Rh synergy in a three-way catalytic converter, *Int. J. Chem. React. Eng.* 11 (535) (2013), <http://dx.doi.org/10.1515/jcre-2013-0072>.
- [2] Z. Hu, F.M. Allen, C.Z. Wan, R.M. Heck, J.J. Steger, R.E. Lakis, C.E. Lyman, Performance and structure of pt-Rh three-way catalysts: mechanism for Pt/Rh synergism, *J. Catal.* 174 (1998) 13–21, <http://dx.doi.org/10.1006/jcat.1997.1954>.
- [3] J.G. Nunan, H.J. Robota, M.J. Cohn, S.A. Bradley, Physicochemical properties of Ce-containing three-way catalysts and the effect of Ce on catalyst activity, *J. Catal.* 133 (1992) 309–324, [http://dx.doi.org/10.1016/0021-9517\(92\)90242-A](http://dx.doi.org/10.1016/0021-9517(92)90242-A).
- [4] B. Choi, K. Lee, LNT-/CDPF catalysts for simultaneous removal of NOx and PM from diesel vehicle exhaust, *Chem. Eng. J.* 240 (2014) 476–486, <http://dx.doi.org/10.1016/j.cej.2013.10.100>.
- [5] W.S. Epling, L.E. Campbell, A. Yezersets, N.W. Currier, J.E. Parks, Overview of the fundamental reactions and degradation mechanisms of NOx storage/reduction catalysts, *Catal. Rev.* 46 (2004) 163–245, <http://dx.doi.org/10.1081/CR-200031932>.
- [6] J. Winterlin, T. Zambelli, J.V. Barth, G. Ertl, Complex pathways in dissociative adsorption of oxygen on platinum, *Nature* 390 (1997) 495–497, <http://dx.doi.org/10.1038/37329>.
- [7] S.J. Teichner, Recent studies in hydrogen and oxygen spillover and their impact on catalysis, *Appl. Catal.* 62 (1990) 1–10, [http://dx.doi.org/10.1016/S0166-9834\(00\)82232-0](http://dx.doi.org/10.1016/S0166-9834(00)82232-0).
- [8] W.C. Conner, J.L. Falconer, Spillover in heterogeneous catalysis, *Chem. Rev.* 95 (1995) 759–788, <http://dx.doi.org/10.1021/cr00035a014>.
- [9] H. Ren, M.P. Humbert, C.A. Menning, J.G. Chen, Y. Shu, U.G. Singh, W.-C. Cheng, Inhibition of coking and CO poisoning of Pt catalysts by the formation of Au/Pt bimetallic surfaces, *Appl. Catal. A: Gen.* 375 (2010) 303–309, <http://dx.doi.org/10.1016/j.apcata.2010.01.018>.
- [10] J. Liu, F.R. Lucci, M. Yang, S. Lee, M.D. Marcinkowski, A.J. Therrien, C.T. Williams, E.C.H. Sykes, M. Flytzani-Stephanopoulos, Tackling CO poisoning with single-atom alloy catalysts, *J. Am. Chem. Soc.* 138 (2016) 6396–6399, <http://dx.doi.org/10.1021/jacs.6b03339>.
- [11] L.M. Baldyga, S.O. Blavo, C.-H. Kuo, C.-K. Tsung, J.N. Kuhn, Size-dependent sulfur poisoning of silica-supported monodisperse Pt nanoparticle hydrogenation catalysts, *ACS Catal.* 2 (2012) 2626–2629, <http://dx.doi.org/10.1021/cs300625m>.
- [12] Z. Yang, N. Zhang, Y. Cao, M. Gong, M. Zhao, Y. Chen, Effect of yttria in Pt/TiO₂ on sulfur resistance diesel oxidation catalysts: enhancement of low-temperature activity and stability, *Catal. Sci. Technol.* 4 (2014) 3032, <http://dx.doi.org/10.1039/C4CY00424H>.
- [13] E. Borfecchia, K.A. Lomachenko, F. Giordanino, H. Falsig, P. Beato, A.V. Soldatov, S. Bordiga, C. Lamberti, Revisiting the nature of Cu sites in the activated Cu-SZ-13 catalyst for SCR reaction, *Chem. Sci.* 6 (2015) 548–563, <http://dx.doi.org/10.1039/C4SC02907K>.
- [14] T. Boningari, D.K. Pappas, P.R. Ettreddy, A. Kotrba, P.G. Smirniotis, Influence of SiO₂ on M/TiO₂ (M = Cu, Mn, and Ce) formulations for low-temperature selective catalytic reduction of NO_x with NH₃: surface properties and key components in relation to the activity of, *Ind. Eng. Chem. Res.* 54 (2015) 2261–2273, <http://dx.doi.org/10.1021/ie504709j>.
- [15] X. Yao, F. Gao, Q. Yu, L. Qi, C. Tang, L. Dong, Y. Chen, NO reduction by CO over CuO/CeO₂ catalysts: effect of preparation methods, *Catal. Sci. Technol.* 3 (2013) 1355, <http://dx.doi.org/10.1039/C3CY20805B>.
- [16] M. Zabilskiy, P. Djinović, E. Tchernychova, O.P. Tkachenko, L.M. Kustov, A. Pintar, Nanoshaped CuO/CeO₂ materials: effect of the exposed ceria surfaces on catalytic activity in N₂ O decomposition reaction, *ACS Catal.* 5 (2015) 5357–5365, <http://dx.doi.org/10.1021/acscatal.5b01044>.
- [17] M. Konsolakis, Recent advances on nitrous oxide (N₂ O) decomposition over non-noble-metal oxide catalysts: catalytic performance, mechanistic considerations, and surface chemistry aspects, *ACS Catal.* 5 (2015) 6397–6421, <http://dx.doi.org/10.1021/acscatal.5b01605>.
- [18] G.G. Jernigan, G.A. Somorjai, Carbon monoxide oxidation over three different oxidation states of copper: metallic copper, copper (I) oxide, and copper (II) oxide – a surface science and kinetic study, *J. Catal.* 147 (1994) 567–577, <http://dx.doi.org/10.1006/jcat.1994.1173>.
- [19] S. Zhang, W. Huang, X. Qiu, B. Li, X. Zheng, S. Wu, Comparative study on catalytic properties for low-temperature CO oxidation of Cu/CeO₂ and CuO/CeO₂ prepared via solvated metal atom impregnation and conventional impregnation, *Catal. Lett.* 80 (2002) 41–46, <http://dx.doi.org/10.1023/A:1015318525080>.
- [20] W. Liu, M. Flytzani-Stephanopoulos, Transition metal-promoted oxidation catalysis by fluorite oxides: a study of CO oxidation over Cu-CeO₂, *Chem. Eng. J. Biochem. Eng. J.* 64 (1996) 283–294, [http://dx.doi.org/10.1016/S0923-0467\(96\)03135-1](http://dx.doi.org/10.1016/S0923-0467(96)03135-1).
- [21] K.N. Rao, P. Venkataswamy, B.M. Reddy, Structural characterization and catalytic evaluation of supported copper-ceria catalysts for soot oxidation, *Ind. Eng. Chem. Res.* 50 (2011) 11960–11969, <http://dx.doi.org/10.1021/ie201474p>.
- [22] Y. Wang, J. Wang, H. Chen, M. Yao, Y. Li, Preparation and NO_x-assisted soot oxidation activity of a CuO/CeO₂ mixed oxide catalyst, *Chem. Eng. Sci.* 135 (2015) 294–300, <http://dx.doi.org/10.1016/j.ces.2015.03.024>.
- [23] A.-P. Jia, S.-Y. Jiang, J.-Q. Lu, M.-F. Luo, Study of catalytic activity at the CuO-CeO₂ interface for CO oxidation, *J. Phys. Chem. C* 114 (2010) 21605–21610, <http://dx.doi.org/10.1021/jp108556u>.
- [24] A. Davó-Quíñones, M. Navlani-García, D. Lozano-Castelló, A. Bueno-López, J.A. Anderson, Role of hydroxyl groups in the preferential oxidation of CO over copper oxide-cerium oxide catalysts, *ACS Catal.* 6 (2016) 1723–1731, <http://dx.doi.org/10.1021/acscatal.5b02741>.
- [25] Q. Liang, X. Wu, D. Weng, H. Xu, Oxygen activation on Cu/Mn-Ce mixed oxides and the role in diesel soot oxidation, *Catal. Today* 139 (2008) 113–118, <http://dx.doi.org/10.1016/j.cattod.2008.08.013>.
- [26] S. Mosconi, I.D. Lick, A. Carrascull, M.I. Ponzi, E.N. Ponzi, Catalytic combustion of diesel soot: Deactivation by SO₂ of copper and potassium nitrate catalysts supported on alumina, 2007. doi:10.1016/j.catcom.2007.01.026.
- [27] B. Zhou, S. Hermans, G.a. Somorjai, Nanotechnol. Catal. (2004), <http://dx.doi.org/10.1007/978-0-387-34688-5>.
- [28] K. Pelzer, M. Hävecker, M. Bouallec, J.-P. Candy, J.-M. Basset, Stabilization of 200-atom platinum nanoparticles by organosilane fragments, *Angew. Chem. Int. Ed.* 52 (2011) 5276–5279, <http://dx.doi.org/10.1002/ange.201008209>.
- [29] K. Pelzer, B. Laleu, F. Lefebvre, K. Philippot, B. Chaudret, J.P. Candy, J.M. Basset, New Ru Nanoparticles Stabilized by Organosilane Fragments, (2004). doi:10.1021/CM049086B.
- [30] M. Bouallec, J.-M. Basset, J.-P. Candy, P. Delichere, K. Pelzer, L. Veyre, C. Thieuleux, Regularly distributed and fully accessible pt nanoparticles in silica pore channels via the controlled growth of a mesostructured matrix around Pt colloids, *Chem. Mater.* 21 (2009) 775–777, <http://dx.doi.org/10.1021/cm803013c>.
- [31] M. Bouallec, J.-M. Basset, J.-P. Candy, V. Caps, J.-C. Jumas, S. Norsic, E.A. Quadrelli, L. Veyre, C. Thieuleux, Single-phase heterogeneous Pt₃Sn catalyst synthesized by room-temperature self-assemble, *ChemCatChem* 4 (2012) 1729–1732, <http://dx.doi.org/10.1002/cctc.201200276>.
- [32] D. Baudouin, C. Szeto, P. Laurent, A. De Mallmann, B. Fenet, L. Veyre, U. Rodemerck, C. Cope, C. Thieuleux, Nickel–Silicide Colloid Prepared under Mild Conditions as a Versatile Ni Precursor for More Efficient CO₂ Reforming of CH₄ Catalysts, (2012) 4–7.
- [33] T. Andana, M. Piumenti, S. Bensaid, L. Veyre, C. Thieuleux, N. Russo, D. Fino, E.A. Quadrelli, R. Pirone, Ceria-supported small Pt and Pt₃Sn nanoparticles for NO_x-assisted soot oxidation, *Appl. Catal. B: Environ.* (2017) (submitted (n.d.)).
- [34] G.R. Rao, B.G. Mishra, Structural, redox and catalytic chemistry of ceria based materials, *Bull. Catal. Soc. India* 2 (2003) 122–134.

[35] S. Damyanova, B. Pawelec, K. Arishtirova, M.V.M. Huerta, J.L.G. Fierro, Study of the surface and redox properties of ceria-zirconia oxides, *Appl. Catal. A: Gen.* 337 (2008) 86–96, <http://dx.doi.org/10.1016/j.apcata.2007.12.005>.

[36] E. Aneggi, M. Boaro, C. de Leitenburg, G. Dolcetti, A. Trovarelli, Insights into the redox properties of ceria-based oxides and their implications in catalysis, *J. Alloys Compd.* 408 (2006) 1096–1102, <http://dx.doi.org/10.1016/j.jallcom.2004.12.113>.

[37] A. Trovarelli, Catalytic properties of ceria and CeO₂–containing materials, *Catal. Rev. 38* (1996) 439–520, <http://dx.doi.org/10.1080/01614949608006464>.

[38] H. He, P. Yang, J. Li, R. Shi, L. Chen, A. Zhang, Y. Zhu, Controllable synthesis, characterization, and CO oxidation activity of CeO₂ nanostructures with various morphologies, *Ceram. Int.* 42 (2016) 7810–7818, <http://dx.doi.org/10.1016/j.ceramint.2016.02.005>.

[39] R. Si, M. Flytzani-Stephanopoulos, Shape and crystal-plane effects of nanoscale ceria on the activity of Au–CeO₂ catalysts for the water–Gas shift reaction, *Angew. Chem.* 120 (2008) 2926–2929, <http://dx.doi.org/10.1002/ange.200705828>.

[40] M. Piumetti, S. Bensaid, N. Russo, D. Fino, Nanostructured ceria-based catalysts for soot combustion: investigations on the surface sensitivity, *Appl. Catal. B: Environ.* 165 (2015) 742–751, <http://dx.doi.org/10.1016/j.apcatb.2014.10.062>.

[41] H.-X. Mai, L.-D. Sun, Y.-W. Zhang, R. Si, W. Feng, H.-P. Zhang, H.-C.L. Liu, C.-H. Yan, Shape-Selective synthesis and oxygen storage behavior of ceria nanopolyhedra, *Nanorods Nanocubes* (2005), <http://dx.doi.org/10.1021/JP055584B>.

[42] E. Aneggi, D. Wiater, C. de Leitenburg, J. Llorca, A. Trovarelli, Shape-dependent activity of ceria in soot combustion, *ACS Catal.* 4 (2014) 172–181, <http://dx.doi.org/10.1021/cs400850r>.

[43] M. Piumetti, T. Andana, S. Bensaid, N. Russo, D. Fino, R. Pirone, Study on the CO oxidation over ceria-based nanocatalysts, *Nanoscale Res. Lett.* 11 (2016) 165, <http://dx.doi.org/10.1186/s11671-016-1375-z>.

[44] G. Vilé, S. Colussi, F. Krumeich, A. Trovarelli, J. Pérez-Ramírez, Opposite face sensitivity of CeO₂ in hydrogenation and oxidation catalysis, *Angew. Chem.–Int. Ed.* 53 (2014) 12069–12072, <http://dx.doi.org/10.1002/anie.201406637>.

[45] T. Andana, M. Piumetti, S. Bensaid, N. Russo, D. Fino, R. Pirone, Nanostructured ceria–praseodymia catalysts for diesel soot combustion, *Appl. Catal. B: Environ.* 197 (2016) 125–137, <http://dx.doi.org/10.1016/j.apcatb.2015.12.030>.

[46] M. Piumetti, T. Andana, S. Bensaid, D. Fino, N. Russo, R. Pirone, Ceria-based nanomaterials as catalysts for CO oxidation and soot combustion: effect of Zr–Pr doping and structural properties on the catalytic activity, *AIChE J.* (2016), <http://dx.doi.org/10.1002/aic.15548>.

[47] P. Sudarsanan, B. Hillary, B. Mallesham, B.G. Rao, M.H. Amin, A. Nafady, A.M. Alsalme, B.M. Reddy, S.K. Bhargava, Designing CuO x Nanoparticle–Decorated CeO₂ Nanocubes for Catalytic Soot Oxidation : Role of the Nanointerface in the Catalytic Performance of Heterostructured Nanomaterials, (2016). doi:10.1021/acs.langmuir.5b04590.

[48] M. Piumetti, S. Bensaid, T. Andana, N. Russo, R. Pirone, D. Fino, Cerium–copper oxides prepared by solution combustion synthesis for total oxidation reactions: from powder catalysts to structured reactors, *Appl. Catal. B: Environ.* 205 (2017) 455–468, <http://dx.doi.org/10.1016/j.apcatb.2016.12.054>.

[49] R. Prasad, G. Rattan, Preparation methods and applications of CuO–CeO₂ catalysts: a short review, *Bull. Chem. React. Eng. Catal.* 5 (2010) 7–30, <http://dx.doi.org/10.9767/bcrec.5.1.774>.

[50] W. Liu, M. Flytzani-Stephanopoulos, Total oxidation of carbon monoxide and methane over transition metal fluorite oxide composite catalysts: I. Catalyst composition and activity, *J. Catal.* 153 (1995) 304–316, <http://dx.doi.org/10.1006/jcat.1995.1132>.

[51] S. Scirè, P.M. Riccobene, C. Crisafulli, Ceria supported group IB metal catalysts for the combustion of volatile organic compounds and the preferential oxidation of CO, *Appl. Catal. B: Environ.* 101 (2010) 109–117, <http://dx.doi.org/10.1016/j.apcatb.2010.09.013>.

[52] H. Zhou, Z. Huang, C. Sun, F. Qin, D. Xiong, W. Shen, H. Xu, Catalytic decomposition of N₂O over CuxCe1–xO_y mixed oxides, *Appl. Catal. B: Environ.* 125 (2012) 492–498, <http://dx.doi.org/10.1016/j.apcatb.2012.06.021>.

[53] M. Zabilskiy, P. Djinović, E. Tchernychova, O.P. Tkachenko, L.M. Kustov, A. Pintar, Nanoshaped CuO/CeO₂ materials: effect of the exposed ceria surfaces on catalytic activity in N₂O decomposition reaction, *ACS Catal.* 5 (2015) 5357–5365, <http://dx.doi.org/10.1021/acscatal.5b01044>.

[54] E.D. Hermes, G.R. Jenness, J.R. Schmidt, Decoupling the electronic, geometric and interfacial contributions to support effects in heterogeneous catalysis, *Mol. Simul.* 41 (2015) 123–133, <http://dx.doi.org/10.1080/08927022.2014.926549>.

[55] A. Uzunoglu, H. Zhang, S. Andreescu, L.A. Stanciu, CeO₂–MO x (M: Zr, Ti, Cu) mixed metal oxides with enhanced oxygen storage capacity, *J. Mater. Sci.* 50 (2015) 3750–3762, <http://dx.doi.org/10.1007/s10853-015-8939-7>.

[56] X. Tang, B. Zhang, Y. Li, Y. Xu, Q. Xin, W. Shen, CuO/CeO₂ catalysts: redox features and catalytic behaviors, *Appl. Catal. A: Gen.* 288 (2005) 116–125, <http://dx.doi.org/10.1016/j.apcata.2005.04.024>.

[57] D. Weng, J. Li, X. Wu, Z. Si, NO_x-assisted soot oxidation over K/CuCe catalyst, *J. Rare Earths* 28 (2010) 542–546, [http://dx.doi.org/10.1016/S1002-0721\(09\)60150-2](http://dx.doi.org/10.1016/S1002-0721(09)60150-2).

[58] X. Wu, Q. Liang, D. Weng, Z. Lu, The catalytic activity of CuO–CeO₂ mixed oxides for diesel soot oxidation with a NO/O₂ mixture, *Catal. Commun.* 8 (2007) 2110–2114, <http://dx.doi.org/10.1016/j.catcom.2007.04.023>.

[59] A. Roussey, *Preparation of Copper-based Catalysts for the Synthesis of Silicon Nanowires*, 1, Université Claude Bernard, Lyon, 2012.

[60] L. Soler, A. Casanovas, C. Escudero, V. Pérez-Dieste, E. Aneggi, A. Trovarelli, J. Llorca, Ambient pressure photoemission spectroscopy reveals the mechanism of carbon soot oxidation in ceria-based catalysts, *ChemCatChem* 8 (2016) 2748–2751, <http://dx.doi.org/10.1002/cctc.201600615>.

[61] G. Grzybek, P. Stelmachowski, S. Gudyka, P. Indyka, Z. Sojka, N. Guillén-Hurtado, V. Rico-Pérez, A. Bueno-López, A. Kotarba, Strong dispersion effect of cobalt spinel active phase spread over ceria for catalytic N₂O decomposition: the role of the interface periphery, *Appl. Catal. B: Environ.* 180 (2016) 622–629, <http://dx.doi.org/10.1016/j.apcatb.2015.07.027>.

[62] J.-C. Dupin, D. Gonbeau, P. Vinatier, A. Levasseur, Systematic XPS studies of metal oxides, hydroxides and peroxides, *Phys. Chem. Chem. Phys.* 2 (2000) 1319–1324, <http://dx.doi.org/10.1039/a908800h>.

[63] J. Stoch, J. Gablankowska-Kukucz, The effect of carbonate contaminations on the XPS O 1s band structure in metal oxides, *Surf. Interface Anal.* 17 (1991) 165–167, <http://dx.doi.org/10.1002/sia.740170308>.

[64] O. Amadine, Y. Essamli, A. Fihri, M. Larzek, M. Zahouily, Effect of calcination temperature on the structure and catalytic performance of copper–ceria mixed oxide catalysts in phenol hydroxylation, *RSC Adv.* 7 (2017) 12586–12597, <http://dx.doi.org/10.1039/C7RA00734E>.

[65] M. Kurnatowska, W. Mista, P. Mazur, L. Kepinski, Nanocrystalline Ce1–xRuxO₂ –microstructure, stability and activity in CO and soot oxidation, *Appl. Catal. B: Environ.* 148 (2014) 123–135, <http://dx.doi.org/10.1016/j.apcatb.2013.10.047>.

[66] M. Balaguer, C.-Y. Yoo, H.J.M. Bouwmeester, J.M. Serra, Bulk transport and oxygen surface exchange of the mixed ionic–electronic conductor Ce1–xTbxO₂–δ (x = 0, 1, 0.2, 0.5), *J. Mater. Chem. A* 1 (2013) 10234, <http://dx.doi.org/10.1039/c3ta11610g>.

[67] W. Liu, M. Flytzani-Stephanopoulos, Total oxidation of carbon–monoxide and methane over transition metal fluorite oxide composite catalysts, *J. Catal.* 153 (1995) 317–332, <http://dx.doi.org/10.1006/jcat.1995.1133>.

[68] S. Saikova, S. Vorobyev, M. Likhatski, A. Romanchenko, S. Erenburg, S. Trubina, Y. Mikhlin, X-ray photoelectron, Cu L3MM Auger and X-ray absorption spectroscopic studies of Cu nanoparticles produced in aqueous solutions: the effect of sample preparation techniques, *Appl. Surf. Sci.* 258 (2012) 8214–8221, <http://dx.doi.org/10.1016/j.apsusc.2012.05.024>.

[69] T. Andana, M. Piumetti, S. Bensaid, N. Russo, D. Fino, R. Pirone, CO and Soot Oxidation over Ce–Zr–P_x Oxide Catalysts, (n.d.). doi:10.1186/s11671-016-1494-6.

[70] Y.L. Zheng, D. Sen Mao, S.S. Sun, G.Y. Fu, Solvothermal synthesis in ethylene glycol and catalytic activity for CO oxidation of CuO/CeO₂ catalysts, *J. Mater. Sci.* 51 (2016) 917–925, <http://dx.doi.org/10.1007/s10853-015-9420-3>.

[71] S.S. Mulla, N. Chen, W.N. Delgass, W.S. Epling, F.H. Ribeiro, NO₂ inhibits the catalytic reaction of NO and O₂ over Pt, *Catal. Lett.* 100 (2005) 267–270, <http://dx.doi.org/10.1007/s10562-004-3466-1>.

[72] S.S. Mulla, N. Chen, L. Cumaranatunge, G.E. Blau, D.Y. Zemlyanov, W.N. Delgass, W.S. Epling, F.H. Ribeiro, Reaction of NO and O₂ to NO₂ on Pt: kinetics and catalyst deactivation, *J. Catal.* 241 (2006) 389–399, <http://dx.doi.org/10.1016/j.jcat.2006.05.016>.